Molecular Therapy
Original Article

IGF1 Treatment Improves Cardiac Remodeling after Infarction by Targeting Myeloid Cells

Andre Heinen,[1] Rianne Nederlof,[1] Priyadarshini Panjwani,[1] André Spychala,[1] Tengis Tschaidse,[1] Heiko Reffelt,[1] Johannes Boy,[1] Annika Raupach,[1] Stefanie Gödecke,[1] Patrick Petzsch,[2] Karl Köhrer,[2] Maria Grandoch,[3] Anne Petz,[3] Jens W. Fischer,[3] Christina Alter,[4] Jelena Vasilevska,[5] Philipp Lang,[5] and Axel Gödecke[1]

[1]Institut für Herz- und Kreislaufphysiologie, Heinrich-Heine-Universität Düsseldorf, 40225 Düsseldorf, Germany; [2]Biologisch-Medizinisches Forschungszentrum (BMFZ), Genomics and Transcriptomics Labor, Heinrich-Heine-Universität Düsseldorf, 40225 Düsseldorf, Germany; [3]Institut für Pharmakologie und Klinische Pharmakologie, Heinrich-Heine-Universität Düsseldorf, 40225 Düsseldorf, Germany; [4]Institut für Molekulare Kardiologie, Heinrich-Heine-Universität Düsseldorf, 40225 Düsseldorf, Germany; [5]Institut für Molekulare Medizin II, Heinrich-Heine-Universität Düsseldorf, 40225 Düsseldorf, Germany

Insulin-like growth factor 1 (IGF1) is an anabolic hormone that controls the growth and metabolism of many cell types. However, IGF1 also mediates cardio-protective effects after acute myocardial infarction (AMI), but the underlying mechanisms and cellular targets are not fully understood. Here we demonstrate that short-term IGF1 treatment for 3 days after AMI improved cardiac function after 1 and 4 weeks. Regional wall motion was improved in ischemic segments, scar size was reduced, and capillary density increased in the infarcted area and the border zone. Unexpectedly, inducible inactivation of the IGF1 receptor (IGF1R) in cardiomyocytes did not attenuate the protective effect of IGF1. Sequential cardiac transcriptomic analysis indicated an altered myeloid cell response in the acute phase after AMI, and, notably, myeloid-cell *Igf1r*$^{-/-}$ mice lost the protective IGF1 function after I/R. In addition, IGF1 induced an M2-like anti-inflammatory phenotype in bone marrow-derived macrophages and enhanced the number of anti-inflammatory macrophages in heart tissue on day 3 after AMI *in vivo*. In summary, modulation of the acute inflammatory phase after AMI by IGF1 represents an effective mechanism to preserve cardiac function after I/R.

INTRODUCTION

Acute myocardial infarction (AMI) as a result of occlusion of a coronary artery results in rapid cardiomyocyte cell death because of insufficient oxygen and nutrient supply. This primary insult triggers a cascade of events that finally lead to cardiac remodeling, including the infarct zone and the remote myocardium. Local cell death, cytokines, chemokines, and other biomolecules acting as damage-associated molecular patterns (DAMPs) trigger an extensive inflammatory response starting with rapid activation of the innate immune system.[1] Myeloid cell-derived neutrophils are the first to be attracted and infiltrate the infarcted myocardium. Degranulation of neutrophils with release of matrix-degrading enzymes, production of reactive oxygen species (ROS), and neutrophil extracellular trap (NET) formation most likely contribute to further myocardial cell death and infarct expansion, which is observed after reperfusion of the infarct zone.[2] Shortly after the onset of neutrophil invasion, pro-inflammatory monocytes and macrophages accumulate in the heart, leading to sustained inflammation accompanied by phagocytosis of cell debris and matrix fragments. Inflammation is finally resolved by anti-inflammatory monocytes and/or macrophages, which induce tissue remodeling and orchestrate the formation of a stable collagen-rich scar, that replaces the viable myocardium and stabilizes the ventricular wall.[3] This event involves the activation of cardiac fibroblasts, which may differentiate to myofibroblasts. The repair processes are further accompanied by angiogenesis, especially in the infarct border zone.[2] Because of the loss of viable myocardium, the non-ischemic remote myocardium undergoes hypertrophy to compensate for the reduced contractile force development after AMI. However, in the chronic setting, adverse cardiac remodeling may result in deterioration of cardiac function with the consequence of heart failure development.

Strategies to improve the outcome after AMI may target either scar size or functional improvement of the remote myocardium. Approaches to regenerate viable myocardium by transplantation or activation of stem and/or progenitor cells or by pushing cardiac myocytes to re-enter the cell cycle are highly promising options that, however, are still in their infancy.[4] Transplantation of various cell types, including myeloid cells, can induce some functional improvement, but, in most cases, the therapeutic benefit is rather due to paracrine factors influencing the healing process. Thus, growth factors, cytokines, and chemokines represent interesting tools to ameliorate myocardial remodeling after AMI.

Insulin-like growth factor 1 (IGF1) is a molecule that might positively influence different aspects of the cardiac remodeling process after AMI. IGF1 is a key regulator of cell proliferation and survival,

Received 24 July 2018; accepted 26 October 2018;
https://doi.org/10.1016/j.ymthe.2018.10.020.

Correspondence: Axel Gödecke, PhD, Institut für Herz- und Kreislaufphysiologie, Heinrich-Heine-Universität Düsseldorf, Universitätsstraße 1, 40225 Düsseldorf, Germany.
E-mail: axel.goedecke@uni-duesseldorf.de

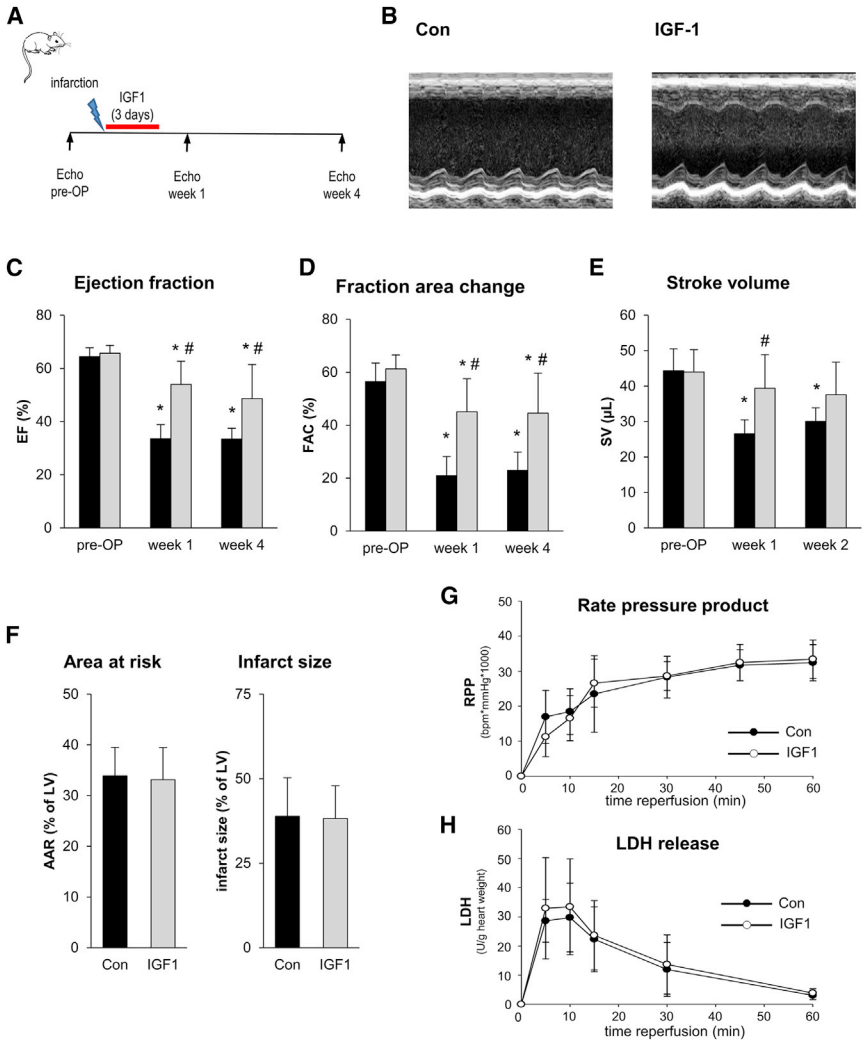

Figure 1. IGF1 Improves Cardiac Function after Myocardial Infarction without Affecting Acute Cardiac Damage

(A) Experimental protocol. C57BL/6J mice were subjected to 45-min LAD coronary artery occlusion and 4 weeks of reperfusion. At the start of reperfusion, mice were treated with IGF1 or vehicle (Con) over 3 days. Echocardiography was performed before I/R (pre-OP [pre-operative]) and 1 and 4 weeks after I/R. (B) Representative parasternal short-axis M-mode views of control (left) and IGF1-treated (right) C57BL/6J mice 4 weeks after myocardial infarction. (C–E) Summarized data for ejection fraction (EF) (C), fraction area change (FAC) (D), and stroke volume (SV) (E) (n = 6 mice for each group). Con, black bars; IGF1, gray bars. (C–E): *p < 0.05 versus pre-OP, #p < 0.05 versus Con (two-way RM ANOVA followed by Tukey's *post hoc* test). (F) Summarized data of *in vivo* analysis of acute myocardial damage. C57BL/6J mice were subjected to 45-min LAD coronary artery occlusion and 2 hr of reperfusion. At the start of reperfusion, mice were treated with IGF1 or vehicle (Con) over 2 hr. Infarct size was determined using 2,3,5-triphenyltetrazolium chloride staining and remote myocardium size by Evans blue staining. The data show no difference in area at risk (AAR) and infarct size between the Con and IGF1 groups (n = 5–6 mice for each group). Con, black bars; IGF1, gray bars; two-tailed unpaired t test. (G and H) For *in vitro* analysis of acute myocardial damage, isolated Langendorff-perfused hearts of C57BL/6J mice underwent 25 min of global ischemia and 1 hr of reperfusion. At the start of reperfusion, hearts were treated with IGF1 (15 nM) or vehicle (Con) during reperfusion. No differences in rate pressure product (G) or LDH release (H) were observed during reperfusion (n = 9–10 hearts for each group). Two-way RM ANOVA followed by Tukey's *post hoc* test. All data are presented as mean ± SD. Additional functional data and the exact p values for each significant difference can be found in Tables S1 and S5.

differentiation, and metabolism. Epidemiologic data show an inverse correlation between IGF1 levels and the occurrence of coronary heart disease (CHD) events, suggesting a protective role of IGF1 in the pathophysiology of CHD, possibly by affecting atherosclerosis progression.[5] Clinical data show that low IGF1 levels are associated with an increased risk of all-cause death and recurrent myocardial infarction.[6] Moreover, there is experimental evidence that IGF1 has cardioprotective properties both in small and large animal models.[7,8] Cardioprotection by IGF1 was impressively demonstrated by cardiac restricted overexpression of the IGF1 propeptide IGF1-Ea, which reduced scar formation in a mouse model with permanent occlusion of the left anterior descending (LAD) coronary artery.[9] This effect was accompanied by preserved cardiac pump function up to 2 months after LAD coronary artery occlusion. However, cardiac hypertrophy and elevated atrial natriuretic peptide (ANP) release already at baseline may be confounders for direct extrapolation of the cardioprotection observed in this model to an IGF1-based therapeutic intervention.

Because chronic overexpression of IGF1 in the heart has no therapeutic relevance, we investigated whether short-term treatment by IGF1 application preserved cardiac pump function after myocardial ischemia and reperfusion (I/R). Moreover, we elucidated the underlying mechanism of protection by using cell-specific IGF1 receptor (IGF1R) knockout mice, which target the IGF1R in cardiomyocytes and in myeloid cells.

RESULTS

IGF1 Improves Cardiac Function after Myocardial Infarction

To assess the influence of IGF1 on the development of contractile function after AMI, mice were treated with IGF1 during the first 3 days after AMI, starting with reperfusion (Figure 1A). Improved left ventricular function 4 weeks after AMI is shown in IGF1-treated animals in representative M-mode traces (Figure 1B). In the control group (Con) without IGF1 treatment, temporary occlusion of the LAD coronary artery caused a reduction of the ejection fraction (EF) by approximately 48% both at week 1 and 4 after MI compared

with pre-AMI values (Figure 1C). The reduction in EF was caused by systolic contractile depression, as seen by an increase in end systolic volume (ESV) rather than by left ventricular dilatation (Table S1). The depressed left ventricular function was also evident as a reduction of fraction area change (FAC). IGF1 application preserved cardiac pump function, as seen by an EF of 53.9% ± 8.7%, which was significantly higher compared with Con animals at the same time point (33.5% ± 5.3%). In line with the effect of IGF1 on EF, FAC (45.1% ± 12.4% IGF1 versus 20.9% ± 7.2% control) and ESV (33.4 ± 6.8 μL IGF1 versus 53.2.5 ± 8.4 μl control) were also improved by IGF1 treatment. The cardio-protective effect of IGF1 was not restricted to 1 week after AMI but was also detected as a similar improvement of functional parameters at week 4 after myocardial ischemia (Figures 1C–1E). Taken together, short-term treatment with IGF1 during the subacute phase after MI caused prolonged improvement in left ventricular function.

IGF1 Does Not Reduce Acute Cardiac Damage after I/R

To investigate whether the protective effect of IGF1 on cardiac function was caused by differences in acute myocardial injury, both *in vivo* and *ex vivo* effects of IGF1 on cardiac damage were determined. *In vivo*, area at risk and acute infarct size were analyzed after 45 min of ischemia followed by 2 hr of reperfusion using standard Evans blue and 2,3,5-triphenyltetrazoliumchlorid (TTC) staining. LAD coronary artery occlusion caused areas at risk (AARs) of comparable sizes in the Con (33.9% ± 5.6%) and IGF1 (33.1% ± 6.3%) group (Figure 1F), and IGF1 treatment did not affect acute infarct size *in vivo* (38.9% ± 11.4% versus 38.2% ± 9.7% of AARs).

To address the effect of IGF1 on acute myocardial damage in isolated hearts, we used 25 min of global cardiac ischemia followed by 2 hr of reperfusion with or without 15 nM IGF1, a concentration that induces approximately half-maximal phosphorylation of the downstream IGF1 target protein kinase B (AKT) (Figure S1A). Administration of IGF1 during the reperfusion phase did not affect cardiac function or cell damage, as seen by no differences in the rate pressure product (Figure 1G) and lactate dehydrogenase (LDH) release (Figure 1H), respectively. Taken together, both *in vivo* and *ex vivo* application of IGF1 had no effect on acute myocardial I/R injury but modulated the cardiac remodeling process during the subacute phase after MI.

IGF1 Improves the Function of the Ischemic Region, Reduces Scar Size, and Promotes Angiogenesis after Myocardial Infarction

In another set of experiments, we focused on cardiac remodeling 1 week after AMI. As shown before, echocardiographic analysis confirmed the beneficial effect of IGF1 on global cardiac function (Figure 2A). An additional regional wall motion analysis (Figure 2B) showed that IGF1 preserved radial displacement, radial strain, and circumferential strain in the anterior free wall segment (i.e., in the ischemic myocardium) while not influencing wall motion and contractility in the remote myocardium (e.g., the posterior septal wall segment) (Figures 2C–2E; Table S2). In line with these findings, histological analysis of these hearts showed that IGF1 caused a reduction in scar size by 37% compared with vehicle-treated control hearts (9.2% ± 4.0% versus 14.7% ± 3.9% of lentiviral vectors [LVs]; Figure 2F). We excluded that this difference in scar size was due to experimental differences such as location of the LAD coronary artery ligation because both groups showed comparable numbers of sectional planes with scars (Figure S2).

Furthermore, analysis of collagen III in the remote myocardium did not show differences between the Con and IGF1 groups, indicating that IGF1 treatment did not affect diffuse cardiac fibrosis (Figure 2G).

Immunohistological analysis of the vascularization 1 week after MI was also performed. In the remote myocardium, we could not detect differences in capillary density, measured as the number of $CD31^+$ vessels of vehicle- or IGF1-treated animals (vehicle, 2,849 ± 232 $CD31^+$ vessels/mm^2; IGF1, 2,905 ± 244 $CD31^+$ vessels/mm^2; Figure 2H). In contrast, vessel numbers were increased in IGF1-treated animals both in the border zone (Figure 2H; vehicle, 1,467 ± 110 $CD31^+$ vessels/mm^2; IGF1, 1,677 ± 72 $CD31^+$ vessels/mm^2; $p < 0.05$) and the scar area (Figure 2H; 495 ± 92 $CD31^+$ vessels/mm^2 versus 654 ± 132 $CD31^+$ vessels/mm^2; $p < 0.05$). No differences were observed in the amount of $CD31^+$ α smooth muscle actin $(\alpha SMA)^+$ cells in any of the three regions (Figure 2H), indicating that the effect of IGF1 is on capillaries and not arterioles.

IGF1 Protects the Heart after AMI Independent of IGF1R Signaling in Cardiomyocytes

Because earlier work demonstrated that IGF1 may affect cardiomyocyte function and survival by numerous mechanisms, including inhibition of apoptosis and altered myocardial microRNA expression,[10] we hypothesized that cardiomyocytes might be the target of the IGF1 effect. To test this hypothesis by genetic means, we conducted experiments in iCM-IGF1RKO mice; i.e., mice with an inducible, cardiomyocyte-restricted deletion of the IGF1R gene (*Igf1r*).[11,12] Compared with WT mice, iCM-IGF1RKO mice did not show differences in cardiac function at baseline (Figure 3; Table S2). Although IGF1 treatment improved cardiac functional parameters such as EF and FAC (Figures 3B–3D; Table S3) in wild-type (WT) mice after AMI as before, we unexpectedly found that IGF1 treatment also preserved these functional parameters in iCM-IGF1RKO mice. These data clearly indicated that IGF1R signaling in cardiomyocytes was dispensable for the protective effect of IGF1 on cardiac remodeling after myocardial infarction.

Myeloid Cell-Restricted Depletion of the IGF1R Abolishes the Protective Effect of IGF1

To obtain insights into the molecular mechanisms and target cell types that were affected by IGF1, we performed a microarray analysis of the infarcted area of vehicle- or IGF1-treated mice on days 1, 2, and 7 after AMI using Agilent 60 K microarrays. Canonical pathway analysis demonstrated that predominantly immune cell-related pathways showed the highest probability of being altered in response to IGF1 treatment on day 1 and day 2 after AMI. Analysis of "diseases and biological functions" that might underlie the improved outcome after

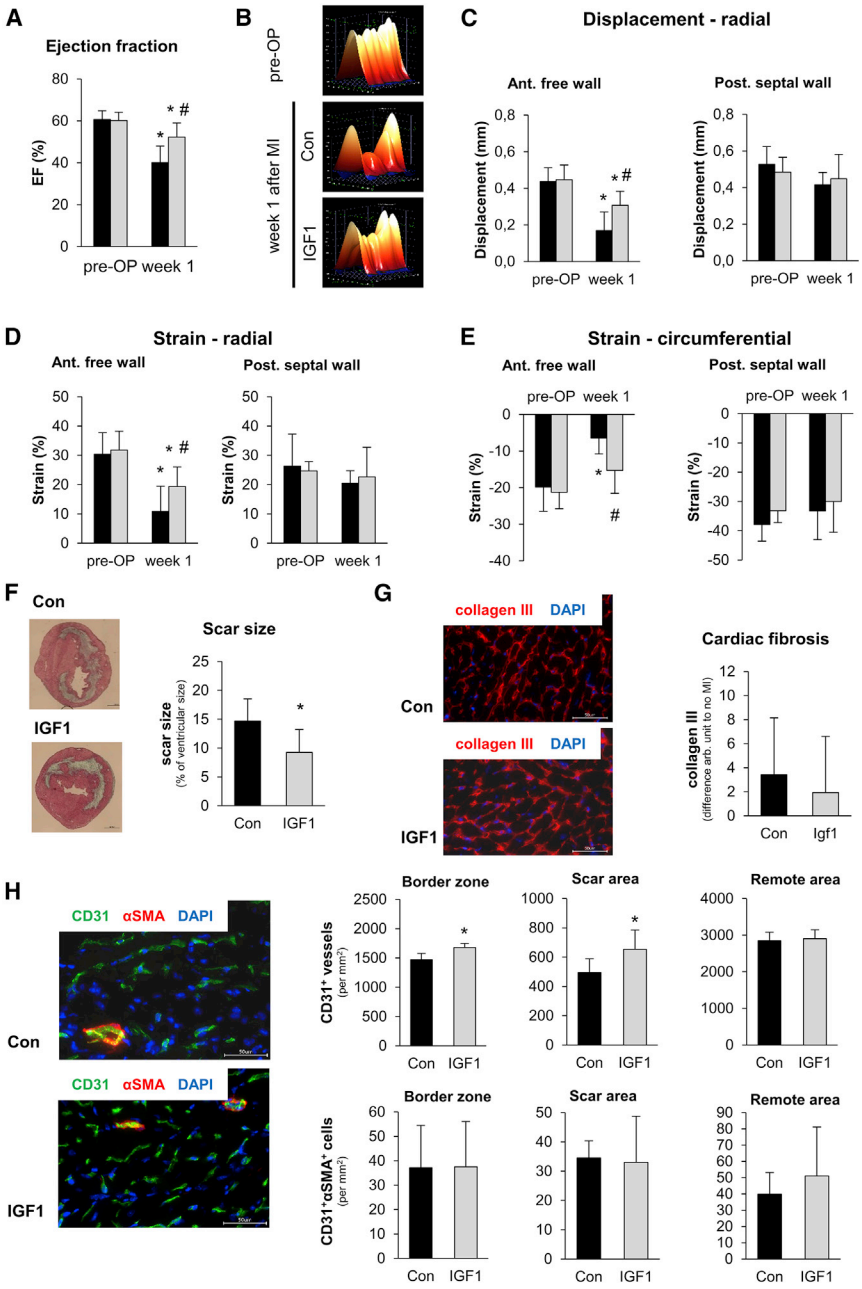

Figure 2. IGF1 Preserves Cardiac Function in the Ischemic Area, Reduces Scar Size, and Increases Capillary Density

C57BL/6J mice were subjected to 45 min of LAD coronary artery occlusion and 1 week of reperfusion. At the start of reperfusion, mice were treated with IGF1 (IGF1, gray bars) or vehicle (Con, black bars) over 3 days. (A) Summarized data for EF before (pre-OP) and 1 week after myocardial infarction. n = 8 mice for each group; *p < 0.05 versus pre-OP, #p < 0.05 versus Con (two-way RM ANOVA followed by Tukey's *post hoc* test). Con, black bars; IGF1, gray bars. (B) Example three-dimensional regional wall displacement illustrations of one cardiac cycle. One example before infarction (top) and two examples 1 week after infarction (with or without IGF1) are shown. (C–E) Summarized data of regional wall motion analysis. Radial endocardial displacement (C), radial strain (D), and circumferential strain (E) are shown for the anterior wall segment (as an example for ischemic myocardium) and the posterior septal wall segment (as an example for remote myocardium). Data of other wall segments can be found in Table S2. *p < 0.05 versus pre-OP, #p < 0.05 versus Con (one-way ANOVA followed by Tukey's *post hoc* test). Con, black bars; IGF1, gray bars. (F) Representative Masson trichrome staining images (left) and summarized data for scar size analysis in hearts 1 week after myocardial infarction. *p < 0.05 versus Con (two-tailed unpaired t test). (G) Representative immunofluorescence images (collagen III, red; DAPI, blue) and summarized data for collagen III content in hearts 1 week after myocardial infarction (two-tailed unpaired t test). Con, black bars; IGF1, gray bars; scale bar, 50 μm. (H) Representative immunofluorescence images of the border zone (CD31, green; αSMA, red; DAPI, blue) and summarized capillary and arteriole density data in the border zone, the scar area, and the remote myocardium (*p < 0.05 versus Con, two-tailed unpaired t test). Con, black bars; IGF1, gray bars; scale bar, 50 μm. Data are presented as mean ± SD. Additional functional data and the exact p value for each significant difference can be found in Tables S2 and S5.

IGF1 treatment consistently identified immunological functions with high negative activation *Z* scores. This indicates that the IGF1-induced alterations in the expression patterns reflected attenuated activation and migration of leukocytes and, in particular, of myeloid cells. These differences were most pronounced on day 1, reduced on day 2, and vanished on day 7 (Figure 4A; Figure S3). This informative result and the importance of myeloid cells invading the heart during the acute and subacute phase after myocardial infarction prompted us to investigate the effect of IGF1 signaling in myeloid cells. For this, we conducted experiments in My-IGF1RKO mice; i.e., mice with monocyte- and/or macrophage- and/or neutrophil-restricted depletion of the IGF1R that were generated by breeding $Igf1r^{fl/fl}$ mice with LysMcre deleters. In these mice, we detected efficient recombination at the *Igf1r* locus in neutrophils as well as monocytes (Figure 4B). On the functional level, My-IGF1RKO mice did not show differences in cardiac function at baseline compared with WT mice (Figure 4; Table S4). After AMI, however, IGF1 had lost its protective effect on cardiac function in My-IGF1RKO mice. As shown by the representative M-mode registration of cardiac function, IGF1 treatment improved contraction of the anterior wall after AMI, which was not detected in IGF1-treated My-IGF1RKO mice (Figure 4C). Quantitative analysis further demonstrated that the elevated EF and FAC caused by IGF1 in WT mice 1 and 4 weeks after AMI was not detectable in My-IGF1RKO

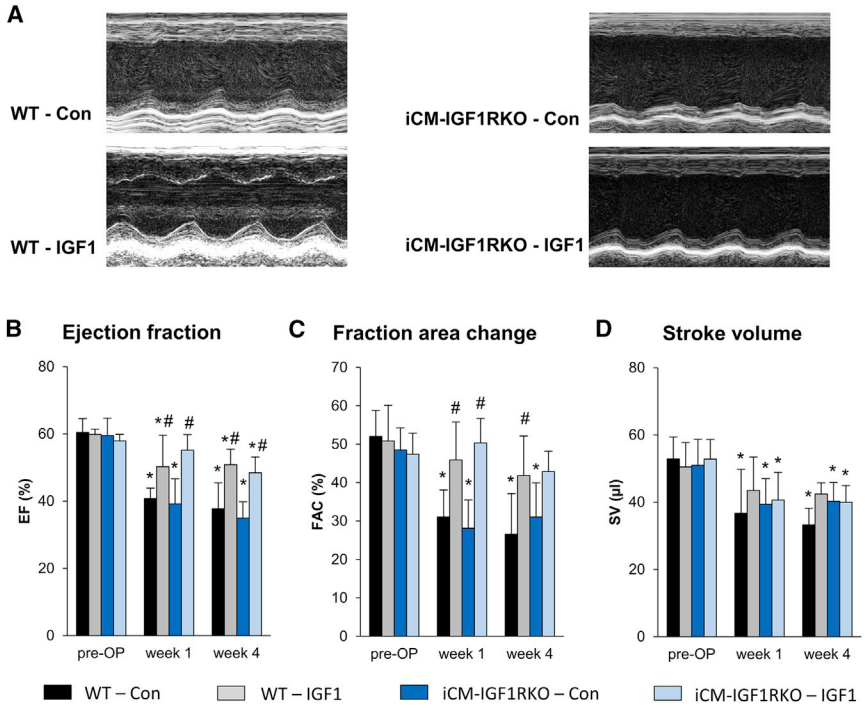

Figure 3. IGF1 Preserves Cardiac Function after Myocardial Infarction Independent of IGF1R Signaling in Cardiomyocytes

Mice with inducible, cardiomyocyte-restricted deletion of the *Igf1r* gene (iCM-IGF1RKO) and wild-type (WT) mice were subjected to 45 min of LAD coronary artery occlusion and 4 weeks of reperfusion. At the start of reperfusion, mice were treated with IGF1 (IGF1) or vehicle (Con) over 3 days. Echocardiography was performed before I/R (pre-OP) and 1 and 4 weeks after I/R. (A) Representative parasternal short-axis M-mode views of Con and IGF1-treated WT and iCM-IGF1RKO mice 4 weeks after myocardial infarction. (B–D) Summarized data for EF (B), FAC (C), and SV (D) (n = 5–6 mice for each group). Data are presented as mean ± SD. *p < 0.05 versus pre-OP, #p < 0.05 versus Con (two-way RM ANOVA followed by Tukey's *post hoc* test). Additional functional data and the exact p value for each significant difference can be found in Tables S3 and S5.

mice (Figures 4D and 4E), indicating that IGF1R signaling in myeloid cells is critically involved in the beneficial effect of IGF1 on cardiac remodeling after myocardial infarction.

IGF1 Affects Macrophage Polarization *In Vitro*

We presumed that IGF1 might exert its beneficial effect by modulation of monocyte and/or macrophage functions that, among the myeloid cells, substantially determine the outcome after MI, either as inflammatory (M1-like subtype) or reparative (M2-like subtype) macrophages.[13] To investigate whether IGF1 influences macrophage polarization *in vitro*, we analyzed the effect of IGF1 on bone marrow-derived cells (BMDCs) according to the protocol depicted in Figure 5A. After mCSF-1-induced macrophage differentiation for 7 days, cells were F4/80$^+$, CD11b$^+$, CD11c$^+$, major histocompatibility complex (MHC) class II$^+$, and Ly6C$^+$ (Figure S4). Interferon γ (IFNγ)/lipopolysaccharide (LPS) treatment led to the induction of an M1-like macrophage phenotype (Figure 5B) characterized by the induction of CD38, which we considered a marker for inflammatory M1-polarized macrophages.[14] In contrast, interleukin-4 (IL-4) and IL-13 induced substantial upregulation of the mannose receptor CD206, indicating an alternatively stimulated M2-like macrophage subtype.[15] When we used IGF1 instead of the "classic" polarizers, we found that IGF1-treated macrophages were also positive for CD206 and negative for CD38. Thus, IGF1 promoted polarization toward an M2-like phenotype (Figures 5B–5D).

This result was further corroborated by qPCR analysis of additional markers of macrophage polarization (Figure 5E). We found that IGF1 induced the expression of the mannose receptor (*Mrc1*), arginase (*Arg1*), and resistin-like α (*Retnla*), similar to IL-4 and IL-13 stimulation. In contrast, IGF1did not induce M1 markers such as tumor necrosis factor α (*Tnf*), interleukin 12A (*Il12a*), and type II nitric oxide (NO) synthase (*Nos2*). We further investigated pro-angiogenic markers and found that addition of IGF1 to macrophages led to an increase in *Igf1* expression to the same level as expressed by M2-like cells but did not have any effect on conventional angiogenic markers like *Vegf* or the recently described myeloid cell-derived factor *Emc10*.[16] Although IGF1 induced polarization toward a M2 phenotype to some extent, it did not affect classic polarization when given in combination with IFN-γ and LPS and IL-4 and IL-10, respectively (Figure 5), because we did not observe the appearance of M2 markers in IFN-γ and LPS-treated BMDCs or an elevated response in IL-4- and IL-13-polarized cells.

IGF1 Treatment Increases CD206$^+$ Macrophages in Cardiac Tissue after AMI *In Vivo*

To investigate the *in vivo* effect of IGF1 on macrophage subtypes, we performed additional experiments, isolating single-cell suspensions from hearts of either vehicle- or IGF1-treated C57BL/6J mice 3 days after myocardial infarction. The gating strategy is outlined in Figure 6A. To correlate our *in vitro* analysis in BMDCs, showing that IGF1 induced CD206$^+$ M2-like macrophage polarization, we used CD206 as a marker to identify reparative macrophages.[17] As shown in Figure 6B, treatment did not significantly affect the number of leukocytes (CD45$^+$), neutrophils (CD11b$^+$ Ly6G$^+$), and macrophages (CD11b$^+$ Ly6G$^-$ F4/80^{hi} CD64$^+$). However, analysis of macrophage subtypes showed that IGF1 substantially increased the mean number of CD206$^+$ macrophages (152,777 ± 13,510 versus 108,071 ± 14,023, p = 0.041) without affecting the number of CD206$^-$ macrophages. Thus, IGF1 shifted the ratio of the cardiac macrophage population after AMI toward a reparative anti-inflammatory state

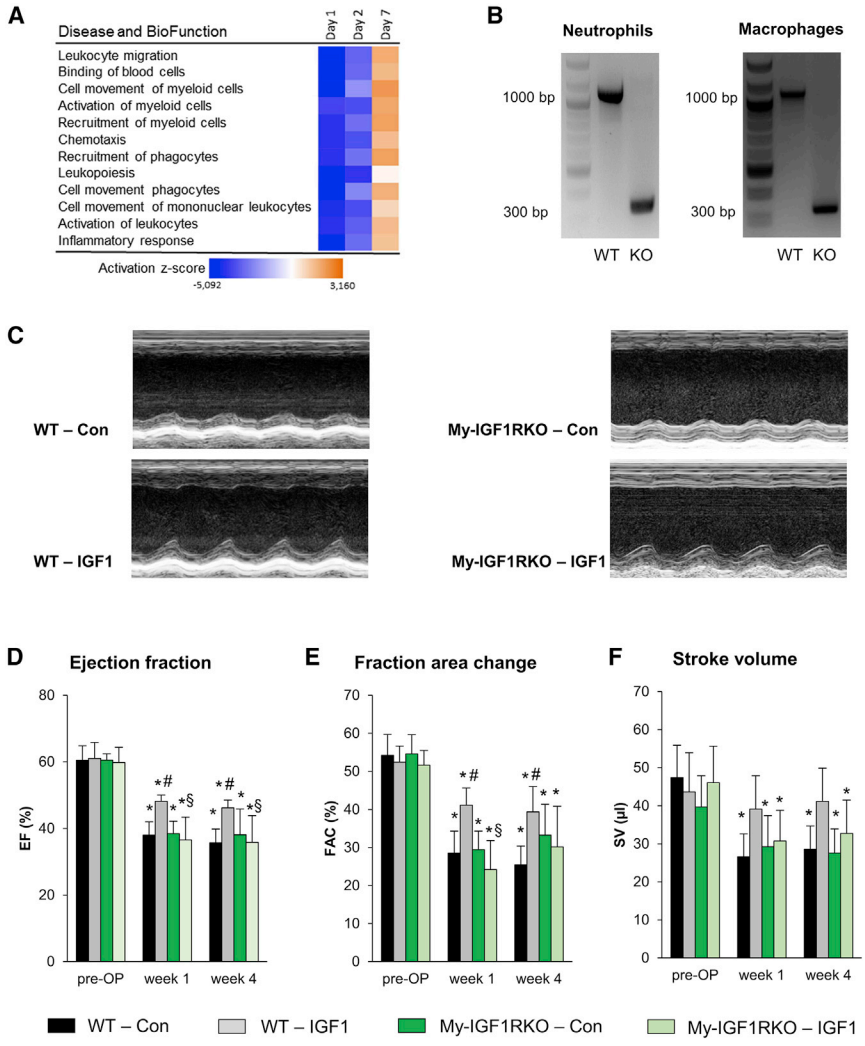

Figure 4. Myeloid Cell-Restricted Deletion of the IGF1R Abolishes the Protective Effect of IGF1

To investigate the role of myeloid cells in the protective IGF1 effect, mice with deletion of the *Igf1r* gene in myeloid cells (My-IGF1RKO) were generated. (A) IGF1 versus BSA activation *Z* scores of the 12 most altered pathways 1, 2, and 7 days after MI from a microarray analysis in C57BL/6J mice. Pathways downregulated in IGF1-treated mice are shown in blue, and upregulation is shown in orange (n = 4 per group). (B) Deletion of the IGF1R gene was verified by PCR. Both neutrophils (left) and macrophages (right) isolated from the bone marrow of WT mice showed the full-length fragment of ~1,000 bp, whereas My-IGF1RKO-derived neutrophils and macrophages solely showed a short fragment of ~300 bp resulting from deletion of the floxed DNA segment. (C) Representative parasternal short-axis M-mode views of Con and IGF1-treated WT and My-IGF1RKO mice 4 weeks after myocardial infarction. (D–F) Summarized data for EF (D), FAC (E), and SV (F) (n = 6–8 mice for each group). Data are presented as mean ± SD. *p < 0.05 versus pre-OP, #p < 0.05 versus WT-Con, §p < 0.05 versus WT-IGF1; two-way RM ANOVA followed by Tukey's *post hoc* test). Additional functional data and the exact p value for each significant difference can be found in Tables S4 and S5.

under *in vivo* conditions. Of note, we also observed a trend toward an increased number of neutrophils ($CD11b^+$ $Ly6G^+$).

DISCUSSION

A major finding of this study is a hitherto unknown dependency of the IGF1-induced improvement of cardiac function after acute myocardial infarction on IGF1R signaling in myeloid cells, whereas IGF1R signaling in cardiomyocytes is dispensable for this effect. In addition, we demonstrate that IGF1 treatment is effective when IGF1 is administered systemically, treatment is started after ischemia, and IGF1 is applied for only 3 days, supporting the translational potential of a short-term IGF1 therapy to reduce adverse cardiac remodeling after cardiac I/R injury.

It is well known that IGF1 plays an important role in normal development and growth.[18] Although IGF1 and its receptors have been extensively studied, there is still increasing interest in the effect of IGF1 in general and, in particular, in cardio-metabolic dysfunction. IGF1 deficiency affects the development of metabolic syndrome[19] and has been described as a risk factor for cardiovascular disease.[5,20] In contrast, high IGF1 levels are associated with a reduction in the relative risk of developing myocardial infarction and for all-combined acute coronary syndromes.[21] In addition to the clinical findings, the beneficial potential of IGF1 is also supported in pre-clinical animal studies. Among others, overexpression of the pre-pro-IGF1-Ea peptide in cardiac myocytes of transgenic mice substantially reduced scar size in combination with preserved cardiac function even after permanent LAD coronary artery ligation.[9] However, despite a clear protective effect in this transgenic model, overexpression of IGF1-Ea is not a therapeutic option, and the mechanism of action remains elusive.

To overcome the limitations of a chronic transgenic approach, we used a 3-day IGF1 infusion protocol, starting the application with reperfusion. Our results demonstrate that this short-term therapy approach with exogenous IGF1 is sufficient to preserve cardiac function in a mouse model with I/R injury. Therefore, IGF1 acts as an early switch to improve the outcome after AMI. Here we clearly show that IGF1 did not affect acute infarct size *in vivo*. Moreover, administration of IGF1 during reperfusion in I/R experiments using the isolated, perfused heart model did not affect left ventricular function or acute cell death. Thus, the long-term improvement in cardiac function by IGF1 was rather due to limiting the infarct expansion that is usually caused by the inflammatory response after reperfusion than

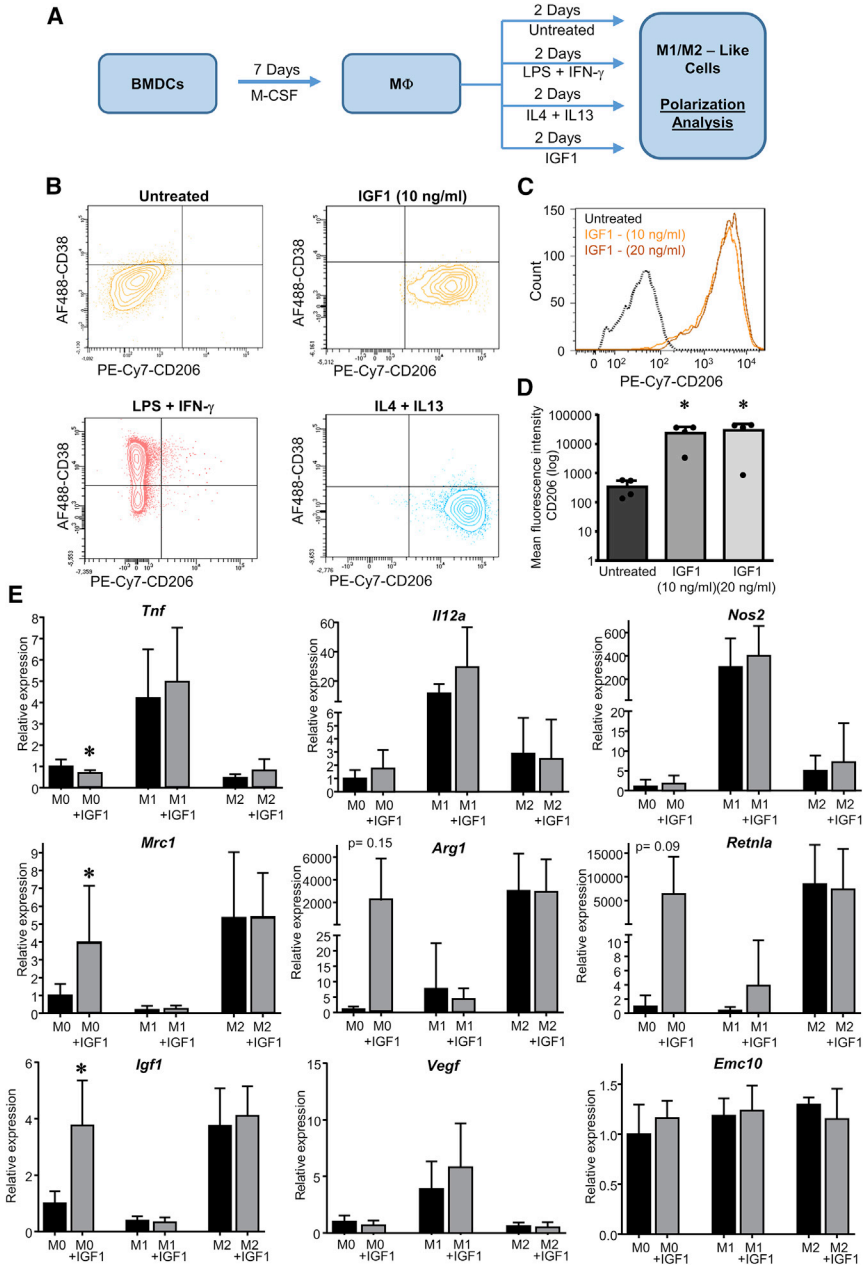

Figure 5. IGF1 Drives Polarization of BMDMs toward an M2-like Phenotype

(A) To investigate the direct effect of IGF1 on macrophages, bone marrow-derived hematopoietic stem cells were cultured in the presence of M-CSF for 7 days. The resulting macrophages were treated for 2 days with IGF1 or the classical polarizers LPS and IFN-γ (M1 polarization) or IL-4 and IL-13 (M2 polarization). (B) Representative fluorescence-activated cell sorting (FACS) plots of cultured macrophages treated with LPS and IFN-γ, IL-4, and IL-13 or IGF1 (10 ng/mL or 20 ng/mL). (C and D) Histogram plot (C) and summarized results (D) for CD206 of untreated or IGF1-treated macrophages. (E) Bone marrow-derived hematopoietic stem cells from WT mice were polarized as described in (A) and treated with or without IGF1. Relative mRNA expression was determined by qPCR for the M1 marker genes *Tnf*, *Il12a*, and *Nos2* (top), the M2 marker genes *Mrc1*, *Arg1*, and *Retnla* (center), and potential protective and/or angiogenic genes *Igf1*, *Vegf*, and *Emc10* (bottom). The results were normalized to β-actin mRNA expression, and x-fold induction was calculated relative to M0 expression. Data are presented as mean ± SD. Only significant results are indicated. In (D), one-way ANOVA followed by Tukey's *post hoc* test was used to compare groups. In (E), two-tailed unpaired t test was used to compare groups. *$p < 0.05$ versus untreated. The exact p value for each significant difference can be found in Table S5.

due to the reduction of the acute infarct size. Also, prior studies have demonstrated that adverse cardiac remodeling can be influenced by exogenous IGF1. As underlying mechanisms, reduced apoptosis and improved remodeling with enhanced vascularization of the infarcted area have been discussed,[7,8,22] but no unambiguous results were presented, which identified the cell type that is the primary target of IGF1 mediating the improved cardiac function after AMI. Notably, in this study, we demonstrate by genetic means that inactivation of the IGF1R on cardiac myocytes did not attenuate the protective function of IGF1, which provides genetic proof that cardiomyocytes are not the direct target in IGF1-mediated cardioprotection.

In search of the cell type being modulated by IGF1, we found, by transcriptomic analysis of the infarct zones, consistent downregulation of pathways involved in inflammation. Functional terms such as "leukocyte migration," "activation of myeloid cells," and related terms had the highest negative *Z* scores and were altered on day 1 and day 2 after AMI. Thus, IGF1 appeared to attenuate myeloid cell function early after AMI so that long-term improvement of cardiac function with smaller scar size occurred. Here we unambiguously show that deletion of the *Igf1r* genes in myeloid cells using the LysMCre deleter results in loss of the cardioprotective effect. Thus, we identified cells of the early immune response as the main target of IGF1 action. The role of IGF1 in modulating inflammation after MI was suggested to contribute to the beneficial effect of chronic high-level IGF1Ea overexpression in cardiomyocytes of transgenic mice.[23] However, this transgenic model has some limitations in terms of IGF1-mediated therapy because sustained overexpression of IGF1Ea results in cardiac hypertrophy and elevated ANP levels,[9] causing different physiological states at the time of LAD coronary artery occlusion. Moreover, elevated IGF1Ea is present in the myocardium before AMI, and, therefore, it remained elusive whether the acute supply of exogenous IGF1 would be effective in cardiac protection.

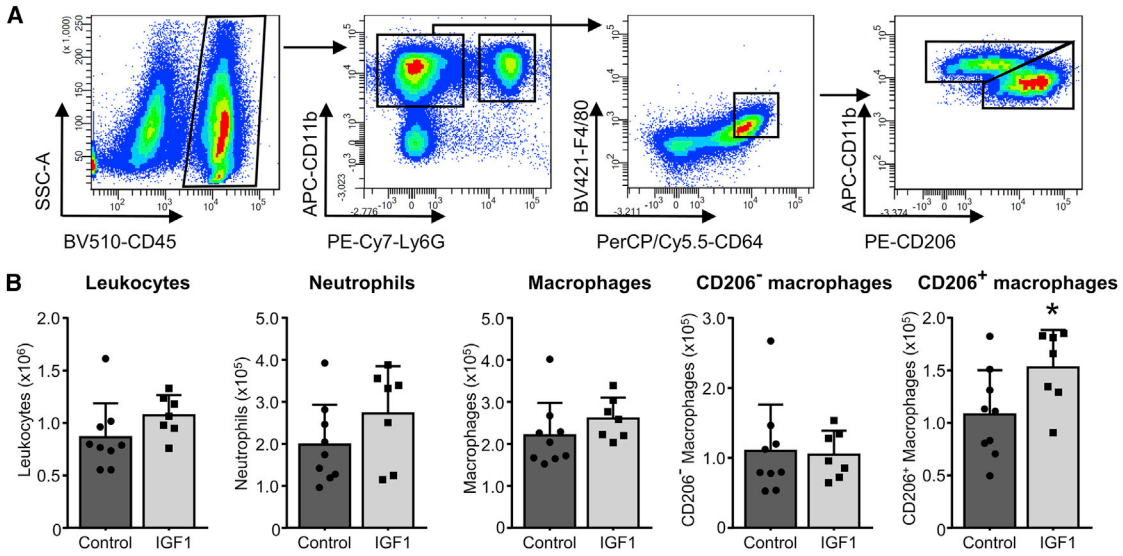

Figure 6. IGF1 Increases Reparative (M2-like) Macrophages in the Heart 3 Days post-MI

C57BL/6J mice were subjected to 45 min of LAD coronary artery occlusion and 3 days of reperfusion. At the start of reperfusion, mice were treated with IGF1 (IGF1, light bars) or vehicle (control, dark bars) over 3 days. (A) A representative FACS gating scheme for the analysis of reparative (M2-like) macrophages, starting after selection of living single cells. (B) IGF1 treatment did not affect the amount of leukocytes ($CD45^+$), neutrophils ($CD11b^+$ $Ly6G^+$), macrophages ($CD11b^+$ $Ly6G^-$ $F4/80^{hi}$ $CD64^+$), or inflammatory (M1-like) macrophages ($CD206^-$) but increased the amount of reparative (M2-like) macrophages ($CD206^+$). n = 7–9. Data are presented as number of cells per heart. Bar graphs represent mean + SD. Two-tailed, unpaired t test was used to compare groups. *$p < 0.05$ versus control. The exact p value for the significant difference can be found in Table S5.

Several experimental findings of our study indicate that the IGF-mediated cardioprotection is mediated by modulation of the macrophage phenotype. We demonstrate that IGF1 drives polarization of BMDCs *in vitro* toward a M2-like phenotype with elevated *CD206*, *Arg1*, and *Retnla* expression, which is similar to that achieved by the classical M2 polarizers IL-4 and IL-13.[24] Thus, these data gave us a clue regarding the potential mechanism underlying the IGF1 effect in that a preferred polarization toward M2-like anti-inflammatory macrophages may induce faster resolution of inflammation with less cell damage occurring during the acute pro-inflammatory response. Moreover, our *in vivo* analysis of macrophage populations in the infarcted hearts of IGF1-treated animals demonstrated a substantial increase in $CD206^+$ macrophages, whereas the numbers of $CD206^-$ macrophages were not altered. This finding clearly supports the proposed mechanism that IGF1 shifts the ratio of pro-inflammatory to anti-inflammatory macrophages toward a more anti-inflammatory, reparative milieu. Although altered numbers of macrophage subtypes may already explain the *in vivo* effects, another level of modulation is, of course, function of IGF1-modulated macrophages. It is well known that many factors can influence the differentiation state of macrophages, with many distinct expression patterns moving the field from the linear M1 and M2 polarization model to a matrix model, which demonstrated a high level of plasticity in macrophage polarization *in vitro*,[25] and by the use of single-cell sequencing *in vivo*.[26] Thus, the precise functional properties of IGF1-modulated macrophages remain elusive and require further investigation.

We also found that IGF1 led to a reduction in infarct size and higher capillary density in the scar region and border zone, which is in line with enhanced repair. IGF1 as a growth factor with angiogenic potential could, of course, directly affect endothelial cells and promote angiogenesis. However, we showed that IGF1-dependent cardioprotection requires IGF1 signaling in myeloid cells, and, therefore, direct stimulation of the endothelium is unlikely. In view of the elevated angiogenesis, we also analyzed *Vegf* expression in IGF1-polarized macrophages, but no effect on *Vegf* expression was found. We assume that IGF1 indirectly, by modulating myeloid cell function, leads to release of an altered set of growth factors, chemokines, and cytokines that, among others, promote angiogenesis.

AMI induces initial infiltration of pro-inflammatory neutrophils and monocytes and/or macrophages, clearing damaged cells and dissolving the extracellular matrix.[3,27] Although our *in vitro* and *in vivo* data point to a critical role of macrophages in IGF1-mediated cardioprotection, we cannot exclude contribution of neutrophils to the IGF1 effect because the LysMcre deleter is also active in neutrophils.[28] Indeed, we confirmed that deletion of the *Igf1r* gene occurred in these cells. Early infiltration of neutrophils with the release of pro-inflammatory cytokines and reactive oxygen species may even enlarge myocardial damage. However, neutrophils also promote the differentiation of monocytes toward reparative anti-inflammatory M2-type macrophages[29] and, thereby, influence the later resolution of inflammation, proliferation of fibroblasts, scar formation, and angiogenesis to stabilize the myocardium and prevent cardiac

rupture.[1] Interestingly, neutrophils can also undergo pro- and anti-inflammatory polarization,[30] although right now, functional subgroups and the diversity of neutrophil populations are much less defined than those of macrophages, and almost nothing is known about neutrophil functional diversity in the heart.[31] In this context, it must be noted that our *in vivo* analysis of immune cell infiltration revealed a trend toward elevated neutrophil numbers in IGF1-treated hearts on day 3 after AMI, a finding that requires further investigation. Therefore, neutrophil- as well as macrophage-specific inactivation of *Igf1r* will be required to dissect the role of each of these myeloid cell types.

For many years, it was assumed that cardiac myocytes must be the primary target of therapeutic interventions after ischemia, but more recent data showed that inflammation substantially drives the remodeling process and affects scar size.[32,33] Therefore, modulation of the inflammatory processes as shown here can be considered a further interesting strategy to ameliorate cardiac remodeling after AMI. In this context, myeloid cells have gained much attention besides their role in driving myocardial inflammation. Many attempts were made to use injection of BMDC populations to improve the functional outcome after myocardial infarction. Indeed, some functional improvement was observed, and the protective role of these cells appears to be the result of paracrine factors that are released from the transplanted cells.[4,34] Indeed, several secreted proteins, such as myeloid cell-derived growth factor (MYDGF) and EMC-10, were discovered. Both are secreted by myeloid cells, protect cardiac myocytes from apoptosis, reduce infarct size, and promote angiogenesis.[16,35] Although we could exclude induction of *Emc10* and *Mydgf* expression by either IGF1 or M1 and M2 polarizers in macrophages, it is conceivable that IGF1, via modulation of the release of growth factors, cytokines, and chemokines from macrophages and, possibly, from neutrophils, shifts the milieu of the infarcted myocardium toward a more reparative state. Therefore, a detailed analysis of the neutrophil and macrophage secretome after IGF1 treatment will give further insight into the mechanism of IGF1-mediated cardioprotection.

Igf1 expression is another hallmark of M2-like macrophages. We also found that IGF1-polarized macrophages elevated *Igf1* expression, which was a further hint of an M2-like polarization induced by IGF1. Thus, the appearance of M2-like cells in the myocardium after AMI appears to create an IGF1-rich milieu. This raises the question of why exogenous IGF1 affected infarct size at all. According to our findings, exogenous IGF1 given during the first 3 days after AMI triggers the enhanced appearance of reparative M2-like macrophages already on day 3 after AMI, a time point when they usually start to increase in number.[36] When present, they may create a sustained IGF1-rich milieu earlier than normal, allowing restriction of IGF1 treatment to the acute phase of inflammation after AMI. Our data underscore findings that modulation of myeloid cells is an effective approach to improve the outcome after AMI and the importance of IGF1 as immune-modulatory cytokine with high translational potential.

MATERIALS AND METHODS

All animal experiments were performed in accordance with the Guide for the Care and Use of Laboratory Animals published by the NIH (NIH publication 85-23, revised 1996). Mice were housed in conventional cages with a 12-hr light and dark cycle and had *ad libitum* access to food and water. All experiments were conducted after approval from the Bezirksregierung Düsseldorf, Germany.

All experiments were performed in a randomized manner, and the analyses of all experimental data were conducted by investigators who where blinded to the treatment protocol.

For this study, C57BL/6J mice (Janvier), tamoxifen-inducible, cardiomyocyte-targeted IGF1R-null mice (iCM-IGF1RKO),[11] or myeloid cell-targeted IGF1R-null mice (My-IGF1RKO) were used. In brief, My-IGF1RKO mice were generated by breeding of LysMCre mice[28] and $Igf1r^{fl/fl}$ mice.[37] Both lines had been backcrossed to C57Bl6/J mice for over 20 generations. Cre-expressing mice were compared with floxed littermates ($Igf1r^{fl/fl}$).

In Vivo Regional Myocardial I/R

In brief, mice were anesthetized with 2% isoflurane, orotracheally intubated, and ventilated with oxygen-enriched gas (40% oxygen) using a rodent ventilator (Minivent microventilator, Hugo Sachs, Germany). Mice were placed in a supine position on a warming plate (Uno, Zevenaar, the Netherlands) to keep body temperature at 37.5°C and received buprenorphine (0.1 mg/kg body weight, subcutaneously [s.c.]) for analgesia. Electrocardiography (ECG) was recorded continuously. After lateral thoracotomy, the pericardium was dissected, and a 7-0 surgical prolene suture was cautiously passed underneath the LAD coronary artery at a position 1 mm from the tip of the left auricle. The suture ends were passed through silicon tubing to form a snare occluder. Myocardial ischemia was produced by tightening the snare and confirmed by blanching of the myocardium and change in ECG (decrease in S wave amplitude). After 45 min, the snare occluder was opened to initiate reperfusion. Afterward, the suture was removed, and the chest was closed. Animals of the IGF1 group received 40 ng/g mature recombinant IGF1 (Miltenyi Biotec, Bergisch Gladbach, Germany) s.c. as a bolus at the start of reperfusion. In addition, IGF1 was administered continuously for the first days of reperfusion (1 μg/g/day) using micro-osmotic pumps (Alzet, 1003D) that were implanted s.c. At the end of the experimental procedures, mice were extubated after they regained spontaneous breathing. Animals received buprenorphine (0.05–0.1 mg/kg body weight, s.c.) every 8 hr for up to 5 days for postoperative analgesia.

Echocardiography

Left ventricular function was analyzed by echocardiography using a Vevo2100 system (Visualsonics) equipped with a 30 MHz linear scanner as described previously.[38] Images were acquired at frame rates consistently above 200 frames/s. Echocardiography was performed before myocardial infarction and 1 and 4 weeks after myocardial infarction. For this, mice were anesthetized with 2% isoflurane and

placed in a supine position on an animal handling platform. ECG and breathing rate were monitored; body temperature was kept at 37°C using a heating system in the handling platform. In addition, an infrared warming lamp was used when required. The linear scanner was placed in a rail-based fixation system that allowed stable fixation of the scanner in all positions. Brightness (B)-mode movies of the parasternal long axis (PSLAX) and three orthogonal short axis (SAX) (mid-ventricular, apical, and basal) were acquired by a blinded investigator, and post-acquisition analysis was performed by the same investigator. For analysis of end diastolic and end systolic volumes, the endocardium of the left ventricle was traced at both diastole and systole. An integrated software tool (Simpson) was used for analysis of ventricular volumes and FAC. EF was calculated using the formula EF = ((EDV − ESV)/EDV) × 100, where EDV is end diastolic volume. Mid-ventricular SAX M-mode was used to determine the systolic (s) and diastolic (d) thickness of the left ventricular anterior wall (LVAW) and posterior (LVPW) wall as well as the left ventricular internal diameter (LVID), and left ventricular mass (LVmass).

Short-axis B-mode cine loops were used for analysis of regional wall motion. Here, radial displacement, longitudinal strain, and radial strain were assessed using the VevoStrain software in accordance with a recently published protocol.[39]

Isolated Mouse Heart Experiments

C57BL/6J mice were injected intraperitoneally with 250 IU heparin. After cervical dislocation, the heart was rapidly excised and transferred for preparation of the aortic trunk to ice-cold Krebs-Henseleit buffer. The aorta was cannulated, and the heart was perfused in non-recirculating Langendorff mode at constant pressure (80 mmHg) with a modified Krebs-Henseleit solution containing 118 mmol/L NaCl, 4.7 mmol/L KCl, 1.2 mmol/L $MgSO_2$, 1.2 mmol/L KH_2PO_4, 25 mmol/L $NaHCO_3$, 0.5 mmol/L EDTA, 2.25 mmol/L $CaCl_2$, 8.32 mmol/L glucose, 1 mmol/L lactate, and 0.1 mmol/L pyruvate, equilibrated with 95% O_2 and 5% CO_2 (pH 7.4, 37°C). A fluid-filled balloon was inserted into the left ventricle, and end-diastolic pressure was set at 3–6 mmHg. Perfusion pressure, coronary flow, and left ventricular developed pressure were measured continuously. Signals were recorded with a sampling rate of 1 kHz using LabChart 7 software (ADInstruments, USA). Hearts were kept at 37°C using a water-heated glass jacket. All hearts underwent a 50-min stabilization period.

To determine a concentration of IGF1 that is sufficient to stimulate IGF1Rs in our isolated heart model, a dose-finding study was performed using the phosphorylation status of AKT as an indicator of the activation of the IGF1 signaling pathway. For this, isolated hearts were perfused after the 50-min stabilization period for 10 min with different concentrations of IGF1 (0, 0.05, 0.5, 5, 15, 50, or 500 nM in 0.1% BSA). At the end of the protocol, hearts were frozen in liquid nitrogen and stored at −80°C for later analysis.

To investigate the effect of IGF1 on cardiac I/R injury, isolated hearts underwent 25 min of global warm ischemia followed by 60 min of reperfusion. IGF1 (15 nM) was administered continuously during the reperfusion period. The coronary effluent was collected at fixed times throughout the protocol (at 5, 10, 15, 30, and 60 min of reperfusion) and stored at −80°C for later determination of LDH leakage as an index of necrosis.

LDH Assay

LDH activity in the effluent was determined as a measure of cell death. It was determined spectrophotometrically by measuring NADH oxidation at 340 nm after addition of pyruvate at 25°C in samples collected at 5, 10, 15, 30, and 60 min of reperfusion according to standard spectrophotometric procedures.[40]

Immunofluorescence and Masson Trichrome Staining

Immunofluorescence staining was performed as described before with slight modifications.[41] Raw hearts were snap-frozen at −40°C and cryo-sectioned at −22°C in short axis orientation. Slices (4 μm) were taken from multiple planes of the complete heart from the apex to the base. The distance between sampled planes was 300 μm (Figures S2A–S2D). Primary antibodies were incubated overnight at 4°C. Secondary antibodies were incubated together for 3 hr at room temperature in the dark. Primary antibodies were as follows: collagen III (ab7778) from Abcam, CD31 (553370) from BD Biosciences, and α-smooth muscle actin (SP6341) from ACRIS. Secondary antibodies were as follows: Cy3 AffiniPure goat anti-rabbit immunoglobulin G (IgG) (111-165-144) and Alexa Fluor 488 AffiniPure goat anti-rat IgG (112-545-167) from Jackson ImmunoResearch Laboratories. The slides were mounted with DAPI Fluoromount-G (SouthernBiotech). Analyses were carried out using a Keyence immunofluorescence microscope (BZ 9000) and ImageJ software.[42]

For analysis of scar size, Masson trichrome staining was performed on cardiac cryosections. For this, sections were incubated for 15 min in Bouin's solution (Sigma-Aldrich), washed, and then incubated with hematoxylin to stain nuclei. After rinsing for 10 min with water, sections were stained for 2 min with acid fuchsin-Ponceau solution (Goldener I) (Morphisto, Frankfurt) and rinsed again with distilled water. Subsequently, the sections were stained for 2 min with phosphomolybdic acid-Orange G solution (Morphisto, Frankfurt) and, after a brief rinse, with Lightgreen solution (Goldener III) (Morphisto, Frankfurt) for 20 min at room temperature, and rinsed again. Then the sections were placed in 1% (v/v) acetic acid for 1 min. Sections were rinsed, dehydrated through alcohol, cleared in xylene (2 × 5 min), and mounted with Entellan (Merck Millipore). Images of the sections were taken with a Keyence BZ 9000 microscope using a 4× objective and the merge function (Keyence). Scar size was analyzed using ImageJ software and is expressed as percent of the ventricular size.

Protein Analysis

For protein analysis, hearts were homogenized in lysis buffer with a tissue raptor (QIAGEN), and protein concentrations were determined with a bicinchoninic acid assay (BCA) protein assay kit (Thermo Scientific). Proteins were separated by SDS-PAGE on polyacrylamide gels and electrotransferred onto Protran nitrocellulose

membranes (GE Healthcare) in a fast blot chamber (Thermo Scientific). Membranes were blocked in Odyssey blocking buffer (LI-COR Biosciences) and analyzed with antibodies against phospho-AKT-Ser^{473} (9271) and AKT (pan) (2920) from Cell Signaling Technology. Secondary antibodies used were α-rabbit or α-mouse IRDye800CW and α-rabbit or α-mouse IRDye680RD from LI-COR Biosciences. Signals were detected and quantified with an Odyssey near-infrared scanner (LI-COR Biosciences).

Total RNA Isolation, cDNA Synthesis, and Microarray Analysis

Total RNA was isolated from heart tissue of the area at risk using the Fibrous Tissue RNeasy Kit (QIAGEN, Hilden, Germany; 74704) according to the manufacturer's instructions and used for array analyses and real-time PCR. In brief, synthesis of cDNA and subsequent fluorescent labeling of cRNA were performed according to the manufacturer's protocol (One-Color Microarray-Based Gene Expression Analysis and Low Input Quick Amp Labeling, Agilent Technologies). Labeled cRNA was hybridized to Agilent SurePrint G3 Mouse GE 8 × 60K microarrays and scanned as described in the manufacturer's' protocol. Signal intensities on 20-bit tiff images were calculated by Feature Extraction software (FE version 12.0.3.2, Agilent Technologies). Probe signal intensities were quantile-normalized across all samples to reduce inter-array variability. Input data preprocessing was concluded by baseline transformation to the median of all samples. Data analyses were conducted with GeneSpring GX software (version 12.5, Agilent Technologies). Differential gene expression was statistically determined by moderated t tests. Microarray data were analyzed using the IPA (Ingenuity Pathway Analysis) software Package (QIAGEN). Microarray data were submitted to the GEO repository (GEO: GSE121779; https://www.ncbi.nlm.nih.gov/geo/).

Isolation of Neutrophils and BMDMs

Neutrophils were isolated from the bone marrow of My-IGF1RKO mice using a neutrophil isolation kit (Miltenyi Biotec) according to the manufacturer's instructions. Bone marrow-derived macrophages (BMDMs) were isolated from the femora and tibiae of C57BL/6J and My-IGF1RKO mice, filtered through a 40-μm filter, and cultured in very low endotoxin (VLE)-DMEM (Merck, Germany, FG1445) supplemented with 10% heat-inactivated fetal calf serum (FCS) in the presence of macrophage colony stimulating factor (M-CSF) (10 ng/mL, PeproTech, 315-02). On day 3, non-adherent cells were discarded, and adherent cells were cultured for an additional 3 days. On day 7, the culture medium was replaced with medium conditioned by the polarizing factors LPS (Sigma, L4391), IFN-γ (Sigma, I4777), IL-4 (PeproTech, 214-14), and IL-13 (PeproTech, 200-13) with or without IGF (Miltenyi Biotech, 130-093-887). 48 h later, the cells were collected and used in subsequent experiments.

Flowcytometry and Real-Time PCR

Cultured BMDM cells were dissociated using cell dissociation buffer (Thermo Fisher, 13150016), washed with Dulbecco's PBS (DPBS) (Thermo Fisher, 14190250), and incubated with Mouse Fc Block (BioLegend, 101302) for 15 min, followed by allophycocyanin (APC)-anti-mouse F4/80 (Thermo Fisher, 17-4801-82), BV605-anti-mouse CD11b (BD Biosciences, 563015), APC-eFluor 780-anti-mouse Ly6C (Thermo Fisher, 47-5932-82), Alexa700-A-anti-mouse MHC class II (Thermo Fisher, 56-5321-82), PerCP-anti-mouse CD11c (Thermo Fisher, 45-0114-82), phycoerythrin (PE)-Cy7-anti-mouse CD206 (macrophage mannose receptor [MMR]) (BioLegend, 141719), and AF488- anti-mouse CD38 (BioLegend, 102714) for 15 min. Isotype control antibodies (BioLegend, eBioscience, and BD Biosciences) were used as the negative control. All cells were washed with PBS before acquisition on a BD LSRFortessa. A gating scheme is depicted in Figure S4.

RNA isolation was performed according to the manufacturer's instructions using TRIzol reagent. cDNA was synthesized from 1 μg RNA using the QuantiTect reverse transcription kit (QIAGEN). qPCR was performed on the Step-One Plus real-time PCR system (Applied Biosystems) with Maxima SYBR Green and ROX qPCR Master Mix (Thermo Scientific). Transcript quantities were normalized to β-actin (*Actb*) mRNA. Gene expression values were calculated relative to unpolarized macrophages. PCR primer sequences are given in Table S6.

For flow cytometric analysis of the heart, C57BL/6J mice were subjected to 45 min of LAD coronary artery occlusion and 3 days of reperfusion. At the start of reperfusion, mice were treated with IGF1 or vehicle over 3 days. A single-cell suspension was obtained via retrograde perfusion with collagenase type I (450 U/mL, Worthington Biochemical, LS004197) and DNAase I (60 U/mL, Roche Diagnostics, 10104159001) in Hank's balanced salt solution (HBSS) (Gibco, 14025). After perfusion, hearts were minced and centrifuged at 300 × *g* for 10 min. The pellet was resuspended in PBS with 0.5% BSA and 2 mM EDTA and filtered over 100-μm and 40-μm filters. To remove cardiomyocytes, the single-cell suspension was centrifuged for 1 min at 50 × *g*. The supernatant was centrifuged for 10 min at 300 × *g*, and the pellet was dissolved in PBS with 0.5% BSA and 2 mM EDTA. Cells were incubated with mouse Fc Block (BioLegend, 101302), fixable viability dye eFluor 780 (eBioscience, 65-0865-14), BV510 anti-mouse CD45 (BD Biosciences, 563891), APC anti-mouse CD11b (BD Biosciences, 553312), PE-Cy7 anti-mouse Ly6G (BD Biosciences, 560601), BV421 anti-mouse F4/80 (BioLegend, 123131), PerCP/Cy5.5 anti-mouse CD64 (BioLegend, 139307), and PE anti-mouse CD206 (BioLegend, 141719). All cells were washed prior to acquisition on a BD FACSCanto II. Data were analyzed using BD FACSDiva software version 8.0.2. A gating scheme is depicted in Figure 6.

Statistical Analysis

All data are presented as mean ± SD. Statistical analysis with the exception of the microarray data was performed using SigmaPlot 13.0 (Systat Software, San Jose, USA). Echocardiographic data were analyzed by two-way repeated measures (RM) ANOVA, followed by Tukey's *post hoc* test. Here, both time effects (within subjects) and group effects (between subjects) were analyzed. Other results were analyzed by either two-tailed unpaired t test or one-way

ANOVA followed by Tukey's *post hoc* test, as appropriate. For all statistical tests, a $p < 0.05$ was considered significant.

SUPPLEMENTAL INFORMATION

Supplemental Information includes four figures and six tables and can be found with this article online at https://doi.org/10.1016/j.ymthe.2018.10.020.

AUTHOR CONTRIBUTIONS

A.G. and A.H. conceived the study, designed the experiments, and supervised the project. A.H., R.N., P.P., A.S., T.T., H.R., S.G., J.B., and A.R. performed the experiments and analyzed the data. K.K. and P.P. performed the microarray analysis. M.G., A.P., J.W.F., and C.A. supported the flow cytometry analysis. J.V. and P.L. supported the myeloid cell isolation and differentiation assay. A.G. and A.H. wrote the manuscript. All authors critically reviewed and approved the manuscript.

CONFLICTS OF INTEREST

The authors declare no competing interests.

ACKNOWLEDGMENTS

The authors thank Julia Albrecht, Daniela Müller, and Susanne Küsters for excellent technical assistance. This work was funded by the German Research Foundation (CRC 1116 "Master Switches in Cardiac Ischemia," TP A06 to A.G.) and the Dr. Sigrid-Worch-Pöhler-Stiftung, Düsseldorf.

REFERENCES

1. Prabhu, S.D., and Frangogiannis, N.G. (2016). The Biological Basis for Cardiac Repair After Myocardial Infarction: From Inflammation to Fibrosis. Circ. Res. *119*, 91–112.
2. Chia, S., Nagurney, J.T., Brown, D.F., Raffel, O.C., Bamberg, F., Senatore, F., Wackers, F.J., and Jang, I.K. (2009). Association of leukocyte and neutrophil counts with infarct size, left ventricular function and outcomes after percutaneous coronary intervention for ST-elevation myocardial infarction. Am. J. Cardiol. *103*, 333–337.
3. Nahrendorf, M., Swirski, F.K., Aikawa, E., Stangenberg, L., Wurdinger, T., Figueiredo, J.L., Libby, P., Weissleder, R., and Pittet, M.J. (2007). The healing myocardium sequentially mobilizes two monocyte subsets with divergent and complementary functions. J. Exp. Med. *204*, 3037–3047.
4. Hodgkinson, C.P., Bareja, A., Gomez, J.A., and Dzau, V.J. (2016). Emerging Concepts in Paracrine Mechanisms in Regenerative Cardiovascular Medicine and Biology. Circ. Res. *118*, 95–107.
5. Juul, A., Scheike, T., Davidsen, M., Gyllenborg, J., and Jørgensen, T. (2002). Low serum insulin-like growth factor I is associated with increased risk of ischemic heart disease: a population-based case-control study. Circulation *106*, 939–944.
6. Bourron, O., Le Bouc, Y., Berard, L., Kotti, S., Brunel, N., Ritz, B., Leclercq, F., Tabone, X., Drouet, E., Mulak, G., et al. (2015). Impact of age-adjusted insulin-like growth factor 1 on major cardiovascular events after acute myocardial infarction: results from the fast-MI registry. J. Clin. Endocrinol. Metab. *100*, 1879–1886.
7. Buerke, M., Murohara, T., Skurk, C., Nuss, C., Tomaselli, K., and Lefer, A.M. (1995). Cardioprotective effect of insulin-like growth factor I in myocardial ischemia followed by reperfusion. Proc. Natl. Acad. Sci. USA *92*, 8031–8035.
8. Kotlyar, A.A., Vered, Z., Goldberg, I., Chouraqui, P., Nas, D., Fridman, E., Chen-Levy, Z., Fytlovich, S., Sangiorgi, G., Spagnoli, L.G., et al. (2001). Insulin-like growth factor I and II preserve myocardial structure in postinfarct swine. Heart *86*, 693–700.
9. Santini, M.P., Tsao, L., Monassier, L., Theodoropoulos, C., Carter, J., Lara-Pezzi, E., Slonimsky, E., Salimova, E., Delafontaine, P., Song, Y.H., et al. (2007). Enhancing repair of the mammalian heart. Circ. Res. *100*, 1732–1740.
10. Iekushi, K., Seeger, F., Assmus, B., Zeiher, A.M., and Dimmeler, S. (2012). Regulation of cardiac microRNAs by bone marrow mononuclear cell therapy in myocardial infarction. Circulation *125*, 1765–73, S1–S7.
11. Moellendorf, S., Kessels, C., Peiseler, L., Raupach, A., Jacoby, C., Vogt, N., Lindecke, A., Koch, L., Brüning, J., Heger, J., et al. (2012). IGF-IR signaling attenuates the age-related decline of diastolic cardiac function. Am. J. Physiol. Endocrinol. Metab. *303*, E213–E222.
12. Shi, L., Kojonazarov, B., Elgheznawy, A., Popp, R., Dahal, B.K., Böhm, M., Pullamsetti, S.S., Ghofrani, H.A., Gödecke, A., Jungmann, A., et al. (2016). miR-223-IGF-IR signalling in hypoxia- and load-induced right-ventricular failure: a novel therapeutic approach. Cardiovasc. Res. *111*, 184–193.
13. Martinez, F.O., Gordon, S., Locati, M., and Mantovani, A. (2006). Transcriptional profiling of the human monocyte-to-macrophage differentiation and polarization: new molecules and patterns of gene expression. J. Immunol. *177*, 7303–7311.
14. Jablonski, K.A., Amici, S.A., Webb, L.M., Ruiz-Rosado, Jde.D., Popovich, P.G., Partida-Sanchez, S., and Guerau-de-Arellano, M. (2015). Novel Markers to Delineate Murine M1 and M2 Macrophages. PLoS ONE *10*, e0145342.
15. Rőszer, T. (2015). Understanding the Mysterious M2 Macrophage through Activation Markers and Effector Mechanisms. Mediators Inflamm. *2015*, 816460.
16. Reboll, M.R., Korf-Klingebiel, M., Klede, S., Polten, F., Brinkmann, E., Reimann, I., Schönfeld, H.J., Bobadilla, M., Faix, J., Kensah, G., et al. (2017). EMC10 (Endoplasmic Reticulum Membrane Protein Complex Subunit 10) Is a Bone Marrow-Derived Angiogenic Growth Factor Promoting Tissue Repair After Myocardial Infarction. Circulation *136*, 1809–1823.
17. Kimbrough, D., Wang, S.H., Wright, L.H., Mani, S.K., Kasiganesan, H., LaRue, A.C., Cheng, Q., Nadig, S.N., Atkinson, C., and Menick, D.R. (2018). HDAC inhibition helps post-MI healing by modulating macrophage polarization. J. Mol. Cell. Cardiol. *119*, 51–63.
18. Butler, A.A., and LeRoith, D. (2001). Minireview: tissue-specific versus generalized gene targeting of the igf1 and igf1r genes and their roles in insulin-like growth factor physiology. Endocrinology *142*, 1685–1688.
19. Aguirre, G.A., De Ita, J.R., de la Garza, R.G., and Castilla-Cortazar, I. (2016). Insulin-like growth factor-1 deficiency and metabolic syndrome. J. Transl. Med. *14*, 3.
20. Janssen, J.A., Stolk, R.P., Pols, H.A., Grobbee, D.E., and Lamberts, S.W. (1998). Serum total IGF-I, free IGF-I, and IGFB-1 levels in an elderly population: relation to cardiovascular risk factors and disease. Arterioscler. Thromb. Vasc. Biol. *18*, 277–282.
21. Ruidavets, J.B., Luc, G., Machez, E., Genoux, A.L., Kee, F., Arveiler, D., Morange, P., Woodside, J.V., Amouyel, P., Evans, A., et al. (2011). Effects of insulin-like growth factor 1 in preventing acute coronary syndromes: the PRIME study. Atherosclerosis *218*, 464–469.
22. O'Sullivan, J.F., Leblond, A.L., Kelly, G., Kumar, A.H., Metharom, P., Büneker, C.K., Alizadeh-Vikali, N., Hristova, I., Hynes, B.G., O'Connor, R., and Caplice, N.M. (2011). Potent long-term cardioprotective effects of single low-dose insulin-like growth factor-1 treatment postmyocardial infarction. Circ. Cardiovasc. Interv. *4*, 327–335.
23. Gallego-Colon, E., Sampson, R.D., Sattler, S., Schneider, M.D., Rosenthal, N., and Tonkin, J. (2015). Cardiac-Restricted IGF-1Ea Overexpression Reduces the Early Accumulation of Inflammatory Myeloid Cells and Mediates Expression of Extracellular Matrix Remodelling Genes after Myocardial Infarction. Mediators Inflamm. *2015*, 484357.
24. Murray, P.J. (2017). Macrophage Polarization. Annu. Rev. Physiol. *79*, 541–566.
25. Xue, J., Schmidt, S.V., Sander, J., Draffehn, A., Krebs, W., Quester, I., De Nardo, D., Gohel, T.D., Emde, M., Schmidleithner, L., et al. (2014). Transcriptome-based network analysis reveals a spectrum model of human macrophage activation. Immunity *40*, 274–288.
26. Cochain, C., Vafadarnejad, E., Arampatzi, P., Pelisek, J., Winkels, H., Ley, K., Wolf, D., Saliba, A.E., and Zernecke, A. (2018). Single-Cell RNA-Seq Reveals the Transcriptional Landscape and Heterogeneity of Aortic Macrophages in Murine Atherosclerosis. Circ. Res. *122*, 1661–1674.
27. Yan, X., Anzai, A., Katsumata, Y., Matsuhashi, T., Ito, K., Endo, J., Yamamoto, T., Takeshima, A., Shinmura, K., Shen, W., et al. (2013). Temporal dynamics of cardiac immune cell accumulation following acute myocardial infarction. J. Mol. Cell. Cardiol. *62*, 24–35.

28. Clausen, B.E., Burkhardt, C., Reith, W., Renkawitz, R., and Förster, I. (1999). Conditional gene targeting in macrophages and granulocytes using LysMcre mice. Transgenic Res. *8*, 265–277.

29. Horckmans, M., Ring, L., Duchene, J., Santovito, D., Schloss, M.J., Drechsler, M., Weber, C., Soehnlein, O., and Steffens, S. (2017). Neutrophils orchestrate post-myocardial infarction healing by polarizing macrophages towards a reparative phenotype. Eur. Heart J. *38*, 187–197.

30. Deniset, J.F., and Kubes, P. (2018). Neutrophil heterogeneity: Bona fide subsets or polarization states? J. Leukoc. Biol. *103*, 829–838.

31. Ma, Y., Yabluchanskiy, A., Iyer, R.P., Cannon, P.L., Flynn, E.R., Jung, M., Henry, J., Cates, C.A., Deleon-Pennell, K.Y., and Lindsey, M.L. (2016). Temporal neutrophil polarization following myocardial infarction. Cardiovasc. Res. *110*, 51–61.

32. Chen, B., and Frangogiannis, N.G. (2017). Immune cells in repair of the infarcted myocardium. Microcirculation *24*, e12305.

33. Sager, H.B., Hulsmans, M., Lavine, K.J., Moreira, M.B., Heidt, T., Courties, G., Sun, Y., Iwamoto, Y., Tricot, B., Khan, O.F., et al. (2016). Proliferation and Recruitment Contribute to Myocardial Macrophage Expansion in Chronic Heart Failure. Circ. Res. *119*, 853–864.

34. Delewi, R., Hirsch, A., Tijssen, J.G., Schächinger, V., Wojakowski, W., Roncalli, J., Aakhus, S., Erbs, S., Assmus, B., Tendera, M., et al. (2014). Impact of intracoronary bone marrow cell therapy on left ventricular function in the setting of ST-segment elevation myocardial infarction: a collaborative meta-analysis. Eur. Heart J. *35*, 989–998.

35. Korf-Klingebiel, M., Reboll, M.R., Klede, S., Brod, T., Pich, A., Polten, F., Napp, L.C., Bauersachs, J., Ganser, A., Brinkmann, E., et al. (2015). Myeloid-derived growth factor (C19orf10) mediates cardiac repair following myocardial infarction. Nat. Med. *21*, 140–149.

36. Troidl, C., Möllmann, H., Nef, H., Masseli, F., Voss, S., Szardien, S., Willmer, M., Rolf, A., Rixe, J., Troidl, K., et al. (2009). Classically and alternatively activated macrophages contribute to tissue remodelling after myocardial infarction. J. Cell. Mol. Med. *13* (9B), 3485–3496.

37. Stachelscheid, H., Ibrahim, H., Koch, L., Schmitz, A., Tscharntke, M., Wunderlich, F.T., Scott, J., Michels, C., Wickenhauser, C., Haase, I., et al. (2008). Epidermal insulin/IGF-1 signalling control interfollicular morphogenesis and proliferative potential through Rac activation. EMBO J. *27*, 2091–2101.

38. Heinen, A., Raupach, A., Behmenburg, F., Hölscher, N., Flögel, U., Kelm, M., Kaisers, W., Nederlof, R., Huhn, R., and Gödecke, A. (2018). Echocardiographic Analysis of Cardiac Function after Infarction in Mice: Validation of Single-Plane Long-Axis View Measurements and the Bi-Plane Simpson Method. Ultrasound Med. Biol. *44*, 1544–1555.

39. Bauer, M., Cheng, S., Jain, M., Ngoy, S., Theodoropoulos, C., Trujillo, A., Lin, F.C., and Liao, R. (2011). Echocardiographic speckle-tracking based strain imaging for rapid cardiovascular phenotyping in mice. Circ. Res. *108*, 908–916.

40. Bergmeyer, H.U. (1974). Methods of enzymatic analysis (Weinheim, Germany: Verlag Chemie).

41. Emde, B., Heinen, A., Gödecke, A., and Bottermann, K. (2014). Wheat germ agglutinin staining as a suitable method for detection and quantification of fibrosis in cardiac tissue after myocardial infarction. Eur. J. Histochem. *58*, 2448.

42. Schindelin, J., Arganda-Carreras, I., Frise, E., Kaynig, V., Longair, M., Pietzsch, T., Preibisch, S., Rueden, C., Saalfeld, S., Schmid, B., et al. (2012). Fiji: an open-source platform for biological-image analysis. Nat. Methods *9*, 676–682.

YMTHE, Volume *27*

Supplemental Information

IGF1 Treatment Improves Cardiac Remodeling after Infarction by Targeting Myeloid Cells

Andre Heinen, Rianne Nederlof, Priyadarshini Panjwani, André Spychala, Tengis Tschaidse, Heiko Reffelt, Johannes Boy, Annika Raupach, Stefanie Gödecke, Patrick Petzsch, Karl Köhrer, Maria Grandoch, Anne Petz, Jens W. Fischer, Christina Alter, Jelena Vasilevska, Philipp Lang, and Axel Gödecke

Figure S1

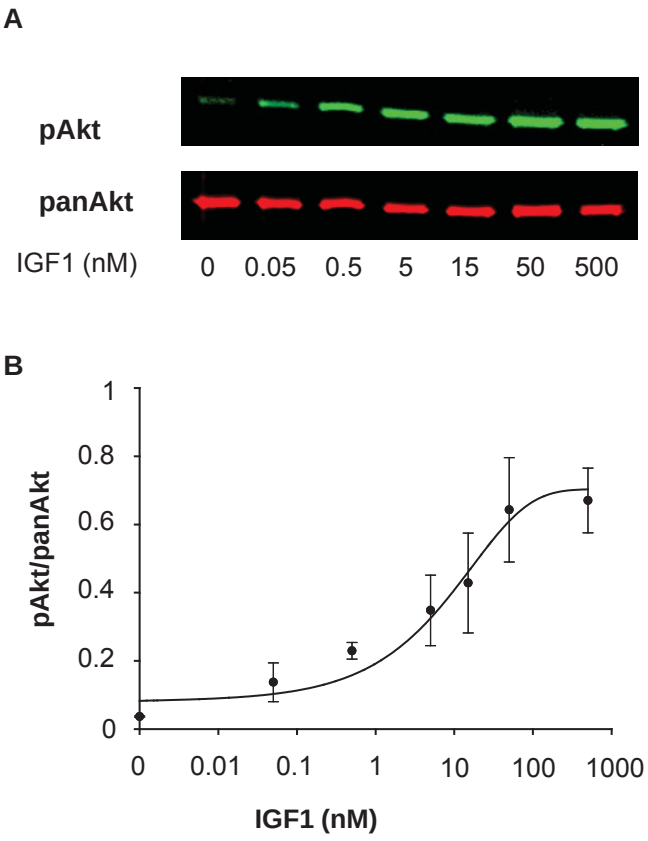
A
pAkt
panAkt
IGF1 (nM)
0 0.05 0.5 5 15 50 500
B
pAkt/panAkt
1
0.8
0.6
0.4
0.2
0
0 0.01 0.1 1 10 100 1000
IGF1 (nM)

Figure S2

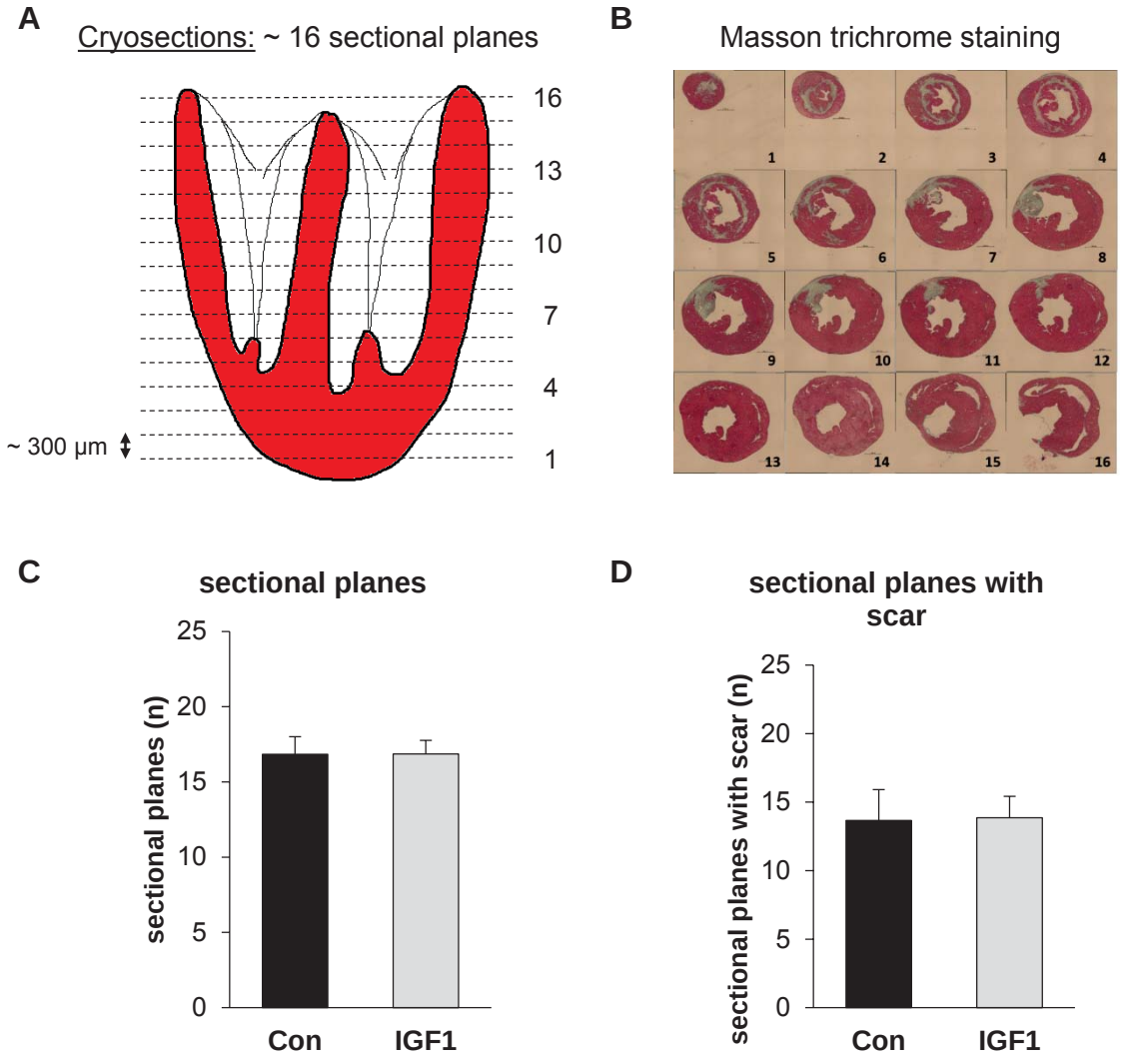
A
Cryosections: ~ 16 sectional planes
16
13
10
7
4
1
~ 300 µm
B
Masson trichrome staining
1
2
3
4
5
6
7
8
9
10
11
12
13
14
15
16
C
sectional planes
sectional planes (n)
25
20
15
10
5
0
Con
IGF1
D
sectional planes with scar
sectional planes with scar (n)
25
20
15
10
5
0
Con
IGF1

Figure S3A

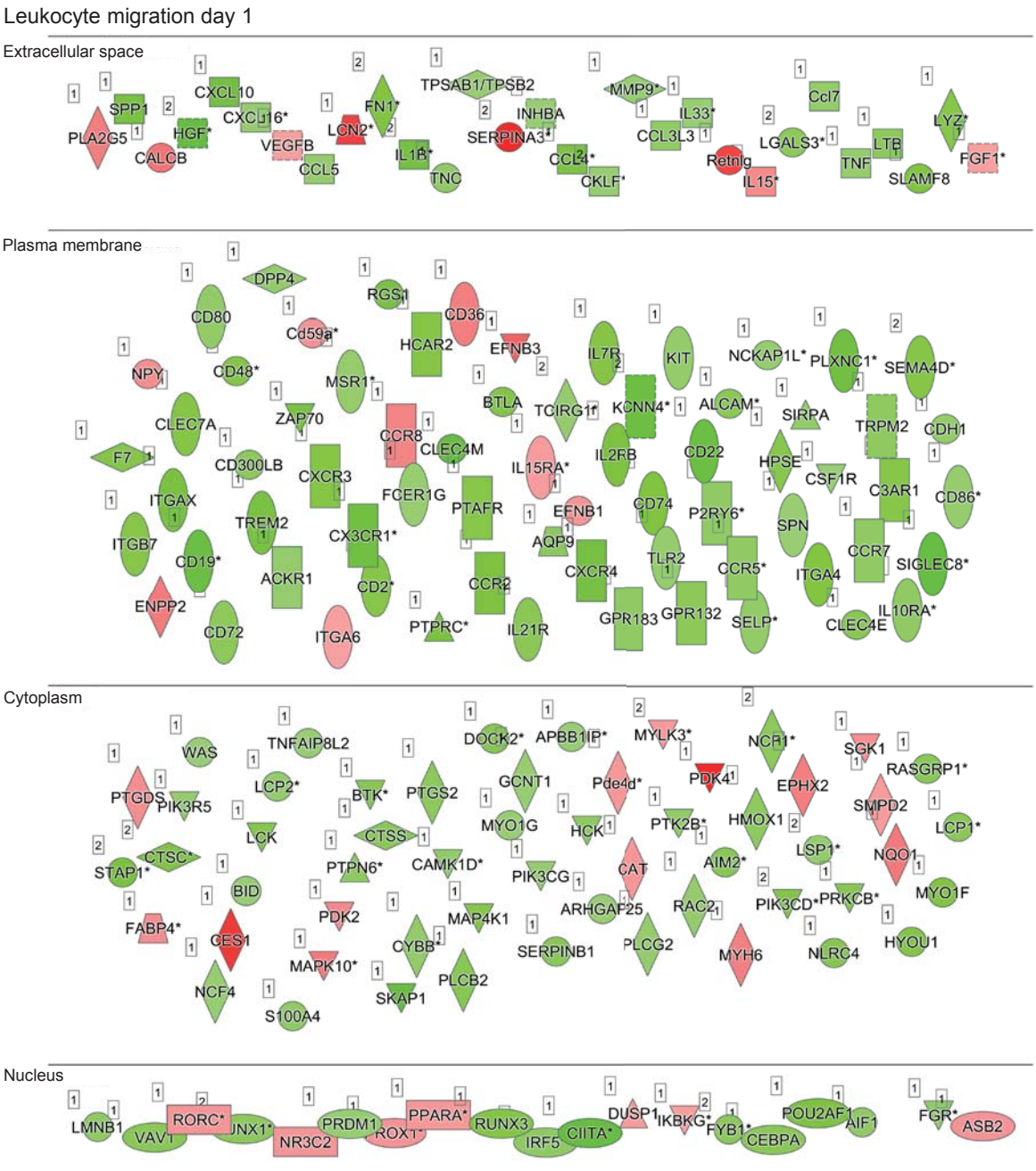
Leukocyte migration day 1
Extracellular space
SPP1
PLA2G5
CALCB
CXCL10
CXCL16*
HGF*
VEGFB
CCL5
FN1*
LCN2*
IL1B*
TNC
TPSAB1/TPSB2
INHBA
SERPINA3*
CCL4*
CKLF*
MMP9*
IL33*
CCL3L3
Retnlg
IL15*
Ccl7
LGALS3*
TNF
LTB
LYZ*
FGF1*
SLAMF8
Plasma membrane
DPP4
CD80
Cd59a*
NPY
CD48*
RGS1
CD36
HCAR2
EFNB3
MSR1*
BTLA
TCIRG1*
IL7R
KIT
KCNN4*
NCKAP1L*
PLXNC1*
SEMA4D*
ALCAM*
SIRPA
TRPM2
CDH1
CLEC7A
ZAP70
CCR8
CLEC4M
F7
CD300LB
CXCR3
FCER1G
PTAFR
IL15RA*
IL2RB
CD22
HPSE
CSF1R
C3AR1
CD86*
ITGAX
TREM2
CX3CR1*
ITGB7
CD19*
ACKR1
CD2*
CCR2
EFNB1
AQP9
CD74
P2RY6*
TLR2
CXCR4
CCR5*
SPN
CCR7
ITGA4
SIGLEC8*
ENPP2
CD72
ITGA6
PTPRC*
IL21R
GPR183
GPR132
SELP*
CLEC4E
IL10RA*
Cytoplasm
WAS
TNFAIP8L2
LCP2*
PTGDS
PIK3R5
LCK
CTSC*
STAP1*
BID
FABP4*
CES1
NCF4
S100A4
BTK*
PTGS2
CTSS
PTPN6*
PDK2
MAPK10*
SKAP1
CYBB*
MAP4K1
PLCB2
CAMK1D*
DOCK2*
APBB1IP*
GCNT1
MYO1G
PIK3CG
ARHGAP25
SERPINB1
MYLK3*
Pde4d*
HCK
CAT
PLCG2
PDK4
PTK2B*
RAC2
MYH6
NCF1*
EPHX2
HMOX1
AIM2*
PIK3CD*
NLRC4
SGK1
SMPD2
LSP1*
PRKCB*
HYOU1
RASGRP1*
LCP1*
NQO1
MYO1F
Nucleus
LMNB1
VAV1
RORC*
JNX1*
NR3C2
PRDM1
ROX1*
PPARA*
RUNX3
IRF5
CIITA*
DUSP1
IKBKG*
FYB1*
CEBPA
POU2AF1
AIF1
FGR*
ASB2

Figure S3B

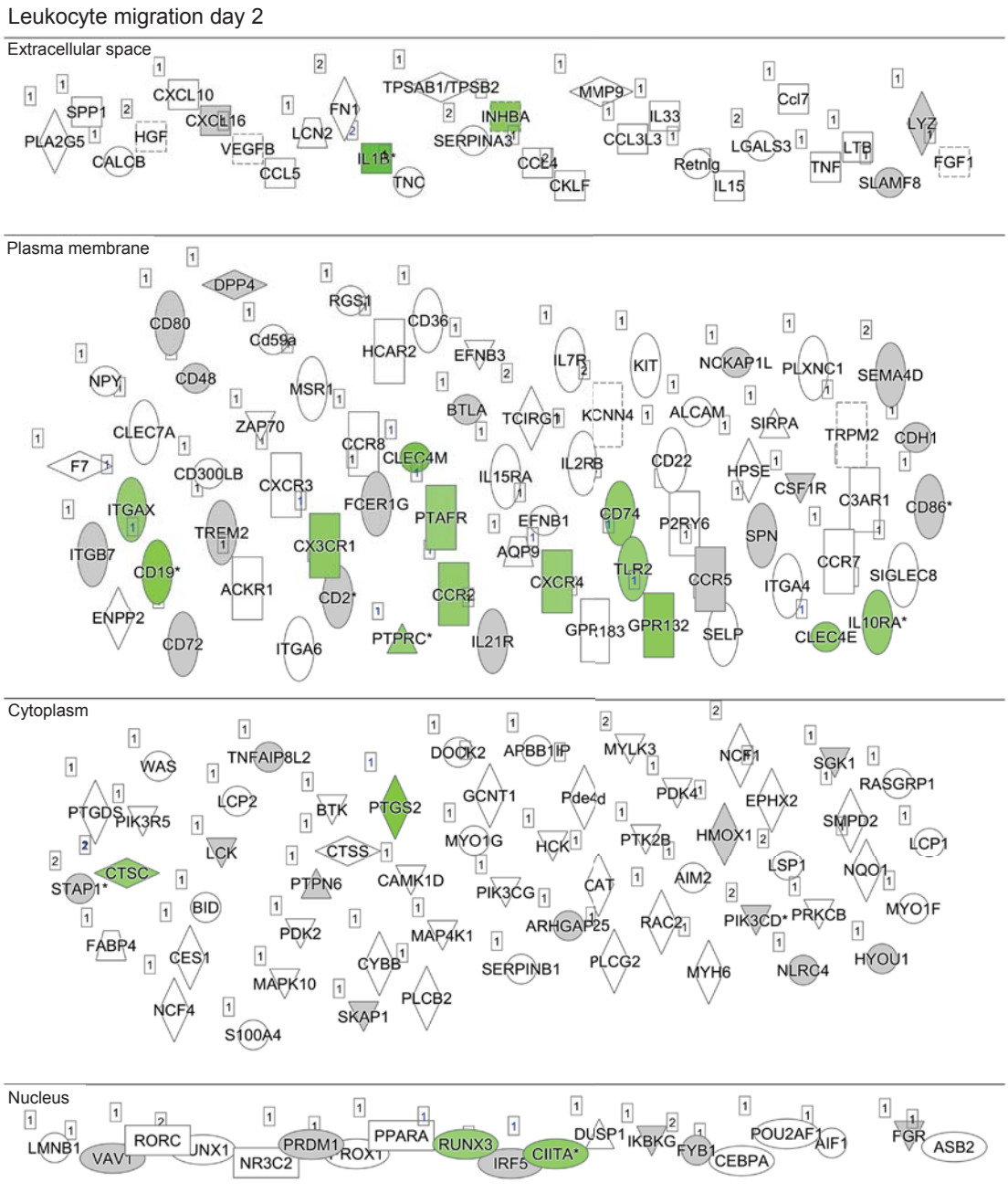
Leukocyte migration day 2
Extracellular space
SPP1
PLA2G5
CALCB
HGF
CXCL10
CXCL16
VEGFB
CCL5
FN1
LCN2
IL1B*
TNC
TPSAB1/TPSB2
INHBA
SERPINA3
MMP9
CCL24
CKLF
IL33
CCL3L3
Retnlg
IL15
Ccl7
LGALS3
TNF
LTB
LYZ
FGF1
SLAMF8
Plasma membrane
DPP4
CD80
Cd59a
NPY
CD48
RGS1
CD36
HCAR2
EFNB3
MSR1
BTLA
TCIRG1
IL7R
KCNN4
KIT
NCKAP1L
PLXNC1
SEMA4D
ALCAM
SIRPA
TRPM2
CDH1
CLEC7A
ZAP70
CCR8
CLEC4M
F7
CD300LB
CXCR3
IL15RA
IL2RB
CD22
HPSE
CSF1R
C3AR1
CD86*
ITGAX
FCER1G
PTAFR
EFNB1
CD74
P2RY6
SPN
TREM2
CX3CR1
AQP9
ITGB7
CD19*
ACKR1
CD2*
CCR2
CXCR4
TLR2
CCR5
CCR7
SIGLEC8
ITGA4
ENPP2
CD72
ITGA6
PTPRC*
IL21R
GPR183
GPR132
SELP
CLEC4E
IL10RA*
Cytoplasm
WAS
TNFAIP8L2
LCP2
PTGDS
PIK3R5
LCK
CTSC
STAP1*
BID
FABP4
CES1
NCF4
S100A4
MAPK10
PDK2
BTK
PTGS2
CTSS
PTPN6
CAMK1D
SKAP1
CYBB
PLCB2
MAP4K1
DOCK2
APBB1IP
GCNT1
MYO1G
PIK3CG
ARHGAP25
SERPINB1
MYLK3
Pde4d
HCK
CAT
PLCG2
PDK4
PTK2B
AIM2
RAC2
MYH6
NCF1
EPHX2
HMOX1
PIK3CD*
NLRC4
SGK1
SMPD2
LSP1
PRKCB
HYOU1
RASGRP1
LCP1
NQO1
MYO1F
Nucleus
LMNB1
VAV1
RORC
JUNX1
NR3C2
PRDM1
ROX1
PPARA
RUNX3
IRF5
CIITA*
DUSP1
IKBKG
FYB1
CEBPA
POU2AF1
AIF1
FGR
ASB2

Figure S3C

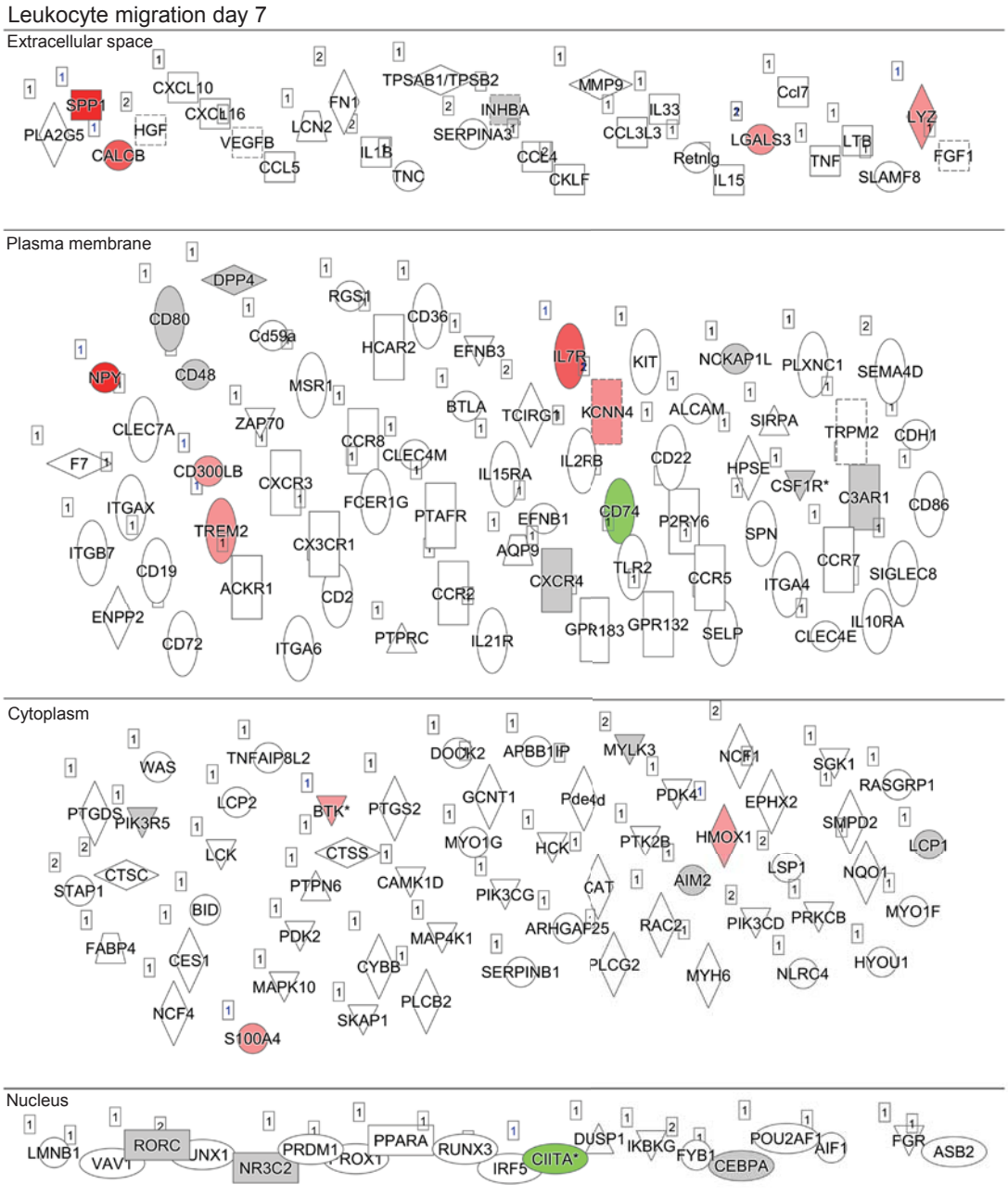
Leukocyte migration day 7
Extracellular space
SPP1
CXCL10
CXCL16
HGF
PLA2G5
CALCB
VEGFB
CCL5
FN1
LCN2
IL1B
TNC
TPSAB1/TPSB2
INHBA
SERPINA3
MMP9
CCL4
CKLF
IL33
CCL3L3
Retnlg
IL15
Ccl7
LGALS3
TNF
LTB
SLAMF8
LYZ
FGF1
Plasma membrane
DPP4
CD80
Cd59a
RGS1
CD36
HCAR2
EFNB3
IL7R
KIT
NCKAP1L
PLXNC1
SEMA4D
NPY
CD48
MSR1
BTLA
TCIRG1
KCNN4
ALCAM
SIRPA
TRPM2
CDH1
CLEC7A
ZAP70
CCR8
CLEC4M
F7
CD300LB
CXCR3
IL15RA
IL2RB
CD22
HPSE
CSF1R*
C3AR1
CD86
ITGAX
FCER1G
PTAFR
EFNB1
CD74
P2RY6
SPN
TREM2
CX3CR1
AQP9
ITGB7
CD19
ACKR1
CD2
CCR2
CXCR4
TLR2
CCR5
CCR7
ITGA4
SIGLEC8
ENPP2
CD72
ITGA6
PTPRC
IL21R
GPR183
GPR132
SELP
CLEC4E
IL10RA
Cytoplasm
WAS
TNFAIP8L2
DOCK2
APBB1IP
MYLK3
NCF1
SGK1
RASGRP1
LCP2
BTK*
PTGS2
GCNT1
Pde4d
PDK4
EPHX2
PTGDS
PIK3R5
MYO1G
HCK
PTK2B
HMOX1
SMPD2
LCP1
LCK
CTSS
CTSC
PTPN6
CAMK1D
PIK3CG
CAT
AIM2
LSP1
NQO1
STAP1
BID
PDK2
MAP4K1
ARHGAP25
RAC2
PIK3CD
PRKCB
MYO1F
FABP4
CES1
CYBB
SERPINB1
PLCG2
MYH6
NLRC4
HYOU1
MAPK10
PLCB2
NCF4
SKAP1
S100A4
Nucleus
LMNB1
VAV1
RORC
JUNX1
NR3C2
PRDM1
ROX1
PPARA
RUNX3
IRF5
CIITA*
DUSP1
IKBKG
FYB1
CEBPA
POU2AF1
AIF1
FGR
ASB2

Figure S4

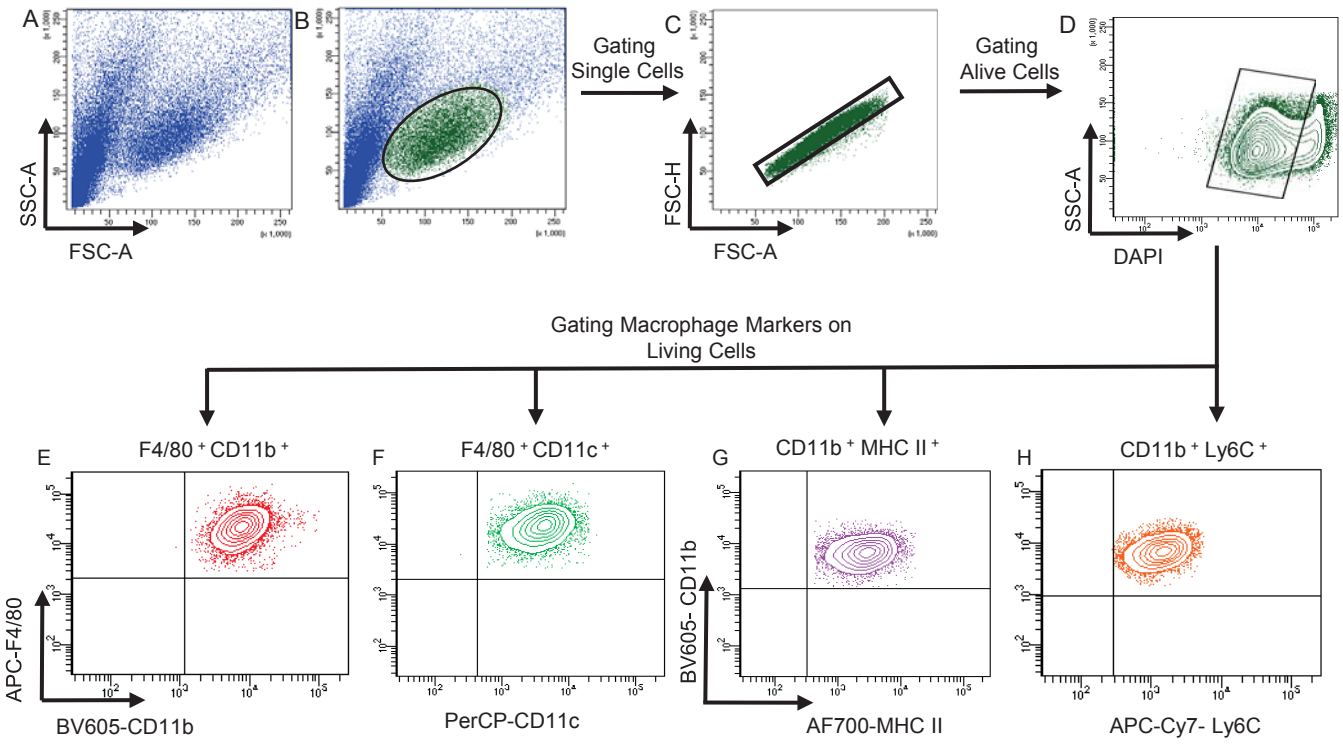
A
SSC-A
FSC-A
B
Gating
Single Cells
C
FSC-H
FSC-A
Gating
Alive Cells
D
SSC-A
DAPI
Gating Macrophage Markers on
Living Cells
E
F4/80 + CD11b +
APC-F4/80
BV605-CD11b
F
F4/80 + CD11c +
PerCP-CD11c
G
CD11b + MHC II +
BV605- CD11b
AF700-MHC II
H
CD11b + Ly6C +
APC-Cy7- Ly6C

Supplemental figure legends

Figure S1 - IGF1 dose response curve

Isolated hearts of mice were perfused for 10 min with indicated concentrations of IGF1.

A IGF1 treatment dose-dependently increases Akt phosphorylation (Ser 473) in isolated hearts of C57Bl/6J mice. Example western blot of phosphoAkt and panAkt.

B Summarized dose response curve of pAkt/panAkt (n = 3 hearts for each concentration).

Data information: Data are presented as mean ± SD.

Figure S2 - Heart cryosection protocol and scar staining

C57Bl/6J mice were subjected to 45 min left anterior descending coronary artery occlusion and 1 week of reperfusion. At the start of reperfusion, mice were treated with IGF1 (IGF1) or vehicle (Con) over three days. Hearts were harvested 1 week after myocardial infarction.

A-B For histological analysis, cryosections (4 μm) were taken from short axis sectional planes (distance 300 μm), and Masson trichrome staining was used to assess scar size.

C-D Summarized data of number of sectional planes (left) and sectional planes with scar (right) (n = 7-8 hearts for each group).

Data information: In (C-D), data are presented as mean ± SD.

Figure S3 - Microarray analysis of the infarct region on days 1, 2 and 7

C57Bl/6J mice were subjected to 45 min left anterior descending coronary artery occlusion, followed by reperfusion. At the start of reperfusion, mice were treated with IGF1 over three days. Agilent microarray analysis of the infarct region was performed on days 1, 2 and 7 after MI. Genes altered in the leukocyte migration pathway (the pathway with the highest change in activity score) are shown on day 1 (Fig S3A), 2 (Fig S3B) and 7 (Fig S3C). Genes downregulated in IGF1 treated animals are shown in green, upregulated genes are shown in red.

Figure S4 - Gating and cell identification using flow cytometer

A Forward and sideward scatter of all the events separated by size and granularity.

B Gating for identification of macrophages separated by size and granularity

C Pulse geometric gate (height and area occupied by cells) for identification of single cells.

D Viability gate for living cells using DAPI.

E-F Living cells positive for F4/80, CD11b and CD11c.

G-H Living cells positive for CD11b, MHCII and Ly6C (low).

Supplemental tables

Table S1: Echocardiographic data of C57Bl/6J mice

pre-OP				
	Con	***p*-value**	**IGF1**	***p*-value**
CO (ml/min)	24.3±3.5		24.2±3.4	
EDV (µl)	68.9±10.0		66.9±9.1	
ESV (µl)	24.6±4.7		23.0±3.7	
LVAW,d (mm)	0.88±0.04		0.78±0.05	
LVAW,s (mm)	1.37±0.03		1.27±0.09	
LVID,d (mm)	3.70±0.22		3.85±0.28	
LVID,s (mm)	2.30±0.27		2.33±0.20	
LVPW,d (mm)	0.74±0.05		0.80±0.16	
LVPW,s (mm)	1.24±0.12		1.27±0.18	
LV mass (mg)	84.7±6.6		86.4±10.3	
Week 1				
	Con	***p*-value**	**IGF1**	***p*-value**
CO (ml/min)	14.9±2.8	< 0.001 *	21.9±3.8	0.005 #
EDV (µl)	79.7±8.7		72.7±9.7	
ESV (µl)	53.2±8.4	< 0.001 *	33.4±6.8	0.003 #
LVAW,d (mm)	1.06±0.09	0.004 *	0.89±0.12	0.004 #
LVAW,s (mm)	1.26±0.18		1.32±0.17	
LVID,d (mm)	4.06±0.26		3.88±0.31	
LVID,s (mm)	3.42±0.30		2.66±0.47	0.010 #
LVPW,d (mm)	0.75±0.12		0.76±0.08	
LVPW,s (mm)	0.93±0.16	0.016 *	1.16±0.13	0.041 #
LV mass (mg)	117.5±25.8	0.016 *	93.0±14.7	0.013 *
Week 4				
	Con	***p*-value**	**IGF1**	***p*-value**
CO (ml/min)	16.4±1.4	0.005 *	21.1±5.2	
EDV (µl)	91.6±16.9	0.015 *	78.7±12.9	
ESV (µl)	61.5±14.6	< 0.001 *	41.2±13.5	< 0.001 * 0.003 #
LVAW,d (mm)	0.85±0.09		0.97±0.09	0.003 *
LVAW,s (mm)	1.08±0.26		1.40±0.16	
LVID,d (mm)	4.46±0.41	< 0.001 *	4.36±0.38	0.013 *
LVID,s (mm)	3.58±0.60	< 0.001 *	3.09±0.58	0.014 *
LVPW,d (mm)	0.79±0.11		0.77±0.08	
LVPW,s (mm)	1.10±0.23		1.20±0.20	
LV mass (mg)	120.8±25.7	0.006 *	126.9±14.2	0.003 *

* = vs. pre-OP; # = vs. Con

Table S2: Regional wall motion analysis

Figure 2C	**Displacement - radial**			
Segment	**group**	**pre-OP**	**week 1**	**p-value**
Lateral wall	Con	0.45±0.09	0.27±0.10	0.002 *
	IGF1	0.41±0.07	0.30±0.11	
Posterior wall	Con	0.47±0.09	0.30±0.12	0.010 *
	IGF1	0.44±012	0.30±0.11	0.035 *
Inferior free wall	Con	0.58±0.08	0.44±0.14	0.032 *
	IGF1	0.52±0.07	0.40±0.13	
Ant. septal wall	Con	0.54±0.07	0.46±0.14	
	IGF1	0.51±0.07	0.50±0.15	
Average	Con	0.49±0.06	0.33±0.09	< 0.001 *
	IGF1	0.47±0.06	0.36±0.08	0.019 *
Figure 2D	**Strain - radial**			
Segment	**group**	**pre-OP**	**week 1**	**p-value**
Lateral wall	Con	23.3±9.8	13.2±14.0	
	IGF1	23.6±6.5	16.2±8.2	
Posterior wall	Con	26.9±10.0	13.7±8.8	0.024 *
	IGF1	28.6±10.4	12.7±10.0	0.006 *
Inferior free wall	Con	31.7±10.7	24.1±10.3	
	IGF1	30.5±9.6	23.0±12.9	
Ant. septal wall	Con	29.2±7.0	25.5±7.9	
	IGF1	28.1±5.3	28.9±10.9	
Average	Con	26.9±6.8	15.3±7.8	0.003 *
	IGF1	25.3±4.0	18.2±6.1	
Figure 2E	**Strain - circumferential**			
Segment	**group**	**pre-OP**	**week 1**	**p-value**
Lateral wall	Con	-22.3±7.7	-10.8±6.5	0.009 *
	IGF1	-22.0±3.9	-13.1±9.2	0.045 *
Posterior wall	Con	-26.4±12.3	-15.4±11.0	
	IGF1	-25.1±10.7	-13.9±4.1	
Inferior free wall	Con	-28.7±5.6	-26.6±10.3	
	IGF1	-23.7±7.7	-21.6±10.4	
Ant. septal wall	Con	-26.2±6.2	-21.4±9.1	
	IGF1	-28.2±7.2	-23.7±9.3	
Average	Con	-25.6±3.4	-16.6±5.3	0.001 *
	IGF1	-24.6±2.7	-17.4±5.1	0.006 *

* = vs. pre-OP

Table S3: Echocardiographic data of iCM-IG1RKO mice

pre-OP					
	WT - Con	**WT - IGF1**	**KO - Con**	**KO - IGF1**	***p*-value**
CO (ml/min)	31.2±3.9	28.3±4.8	28.8±4.8	29.6±1.9	
EDV (µl)	87.7±10.2	84.6±13.3	86.2±14.3	91.3±10.4	
ESV (µl)	34.8±5.9	34.1±6.2	35.2±9.4	38.4±5.1	
LVAW,d (mm)	0.81±0.11	1.06±0.15	0.91±0.09	0.96±0.11	
LVAW,s (mm)	1.24±0.12	1.54±0.15	1.35±0.05	1.38±0.15	
LVID,d (mm)	4.30±0.16	4.08±0.37	4.12±0.27	4.19±0.30	
LVID,s (mm)	2.97±0.20	2.54±0.50	2.74±0.37	2.74±0.29	
LVPW,d (mm)	0.77±0.05	0.84±0.09	0.73±0.07	0.72±0.12	
LVPW,s (mm)	1.25±0.09	1.33±0.14	1.19±0.14	1.25±0.13	
LV mass (mg)	106.1±8.8	108.8±12.9	101.7±16.2	110.8±19.3	
Week 1					
	WT - Con	**WT - IGF1**	**KO - Con**	**KO - IGF1**	***p*-value**
CO (ml/min)	19.9±6.5 *	23.7±5.1	20.9±2.8	22.3±3.9	WT-Con: < 0.001 * KO-Con: 0.002 * KO-IGF1: 0.009 *
EDV (µl)	89.7±28.8	85.9±7.5	100.9±5.7	73.0±8.9	
ESV (µl)	53.0±16.4	42.4±6.6	61.5±9.3	32.4±2.4	WT-Con: 0.022 * KO-Con: < 0.001 * KO-IGF1: 0.006 #
LVAW,d (mm)	0.93±0.15	1.03±0.13	0.88±0.14	0.93±0.03	
LVAW,s (mm)	1.37±0.23	1.40±0.14	1.15±0.26	1.32±0.09	
LVID,d (mm)	4.48±0.41	3.95±0.33	4.68±0.28	3.72±0.27	KO-Con: 0.015 * KO-IGF1: < 0.001 #
LVID,s (mm)	3.33±0.52	2.72±0.46	3.64±0.49	2.46±0.25	KO-Con: 0.002 * KO-IGF1: 0.001 #
LVPW,d (mm)	0.78±0.15	0.91±0.13	0.77±0.14	0.71±0.09	
LVPW,s (mm)	1.06±0.18	1.34±0.16	1.09±0.17	1.17±0.11	WT-Con: 0.041 * WT-IGF1: 0.016 #
LV mass (mg)	128.9±24.9	126.4±28.4	130.7±26.1	87.7±5.8	KO-Con: 0.047 * KO-IGF1: 0.021 #
Week 4					
	WT - Con	**WT - IGF1**	**KO - Con**	**KO - IGF1**	***p*-value**
CO (ml/min)	17.5±2.4 *	23.4±2.5	20.9±3.5	21.1±3.4	WT-Con: 0.001 * WT-IGF1: 0.040 * KO-Con: 0.002 * KO-IGF1: 0.003*
EDV (µl)	94.9±34.1	84.1±9.9	116.4±17.3	82.9±10.1	KO-Con: < 0.001 *
ESV (µl)	61.7±31.6	41.7±8.1	76.2±15.0	42.9±7.4	WT-Con: 0.003 * KO-Con: < 0.001 * KO-IGF1: 0.001 #
LVAW,d (mm)	0.90±0.14	1.08±0.22	0.86±0.17	0.99±0.10	
LVAW,s (mm)	1.21±0.17	1.46±0.26	1.09±0.28	1.35±0.06	
LVID,d (mm)	4.43±0.54	4.16±0.34	4.84±0.25	4.13±0.32	KO-Con: 0.002 * KO-IGF1: 0.011 #
LVID,s (mm)	3.39±0.68	2.94±0.43	3.87±0.45	3.02±0.28	KO-Con: < 0.001 * KO-IGF1: 0.024 #
LVPW,d (mm)	0.79±0.11	0.85±0.07	0.74±0.17	0.80±0.13	
LVPW,s (mm)	1.11±0.15	1.20±0.09	1.01±0.21	1.16±0.09	
LV mass (mg)	125.6±34.8	125.7±21.5	124.4±27.0	116.0±5.8	

* = vs. pre-OP; # = vs. Con

Table S4: Echocardiographic data of My-IG1RKO mice

pre-OP					
	WT - Con	**WT - IGF1**	**KO - Con**	**KO - IGF1**	***p*-value**
CO (ml/min)	25.9±6.7	23.5±5.7	20.2±5.3	24.7±6.4	
EDV (µl)	79.2±17.3	71.1±14.7	66.0±15.0	77.7±18.0	
ESV (µl)	31.8±39.8	27.5±6.0	26.3±7.0	31.6±9.3	
LVAW,d (mm)	0.91±0.05	0.82±0.07	0.83±0.07	0.88±0.07	
LVAW,s (mm)	1.31±0.16	1.24±0.05	1.26±0.15	1.24±0.06	
LVID,d (mm)	3.82±0.39	3.85±0.29	3.71±0.35	3.94±0.57	
LVID,s (mm)	2.48±0.41	2.54±0.35	2.46±0.38	2.76±0.86	
LVPW,d (mm)	0.82±0.08	0.75±0.03	0.81±0.08	0.76±0.09	
LVPW,s (mm)	1.22±0.05	1.19±0.15	1.13±0.11	1.14±0.18	
LV mass (mg)	93.1±17.2	86.8±13.7	84.7±17.6	90.2±15.8	
Week 1					
	WT - Con	**WT - IGF1**	**KO - Con**	**KO - IGF1**	***p*-value**
CO (ml/min)	14.4±3.6	22.5±5.5	15.4±4.5	16.7±4.9	WT-Con: < 0.001 * KO-Con: 0.042 * KO-IGF1: < 0.001*
EDV (µl)	70.8±17.3	81.1±17.1	75.3±16.0	89.9±38.1	
ESV (µl)	44.1±12.0	41.9±8.6	46.1±8.7	59.2±30.9	WT-IGF1: 0.025 * KO-Con: < 0.001 * KO-IGF1: < 0.001 *
LVAW,d (mm)	1.05±0.14	0.97±0.10	0.89±0.11	1.01±0.11	WT-Con: 0.045 * WT-IGF1: 0.023 * KO-IGF1: 0.043 *
LVAW,s (mm)	1.36±0.19	1.29±0.11	1.24±0.13	1.25±0.13	
LVID,d (mm)	3.82±0.60	4.05±0.49	4.09±0.50	4.09±0.68	KO-Con: 0.041 *
LVID,s (mm)	2.80±0.56	2.97±0.61	3.08±0.62	3.28±0.89	KO-Con: 0.007 * KO-IGF1: 0.024 *
LVPW,d (mm)	0.83±0.07	0.82±0.08	0.78±0.10	0.79±0.11	
LVPW,s (mm)	1.09±0.14	1.15±0.09	1.06±0.16	1.03±0.15	
LV mass (mg)	108.2±26.1	113.3±24.8	108.6±36.6	124.4±37.6	WT-IGF1: 0.036 * KO-Con: 0.042 * KO-IGF1: 0.003 *

continued

continuation **Table S4**

Week 4					
	WT - Con	**WT - IGF1**	**KO - Con**	**KO - IGF1**	***p*-value**
CO (ml/min)	14.7±3.3	22.8±4.2	14.5±2.7	18.8±5.5	WT-Con: < 0.001 * KO-Con: 0.014 * KO-IGF1: 0.018 *
EDV (µl)	79.8±11.3	88.6±16.0	73.7±16.2	95.8±33.1	WT-IGF1: 0.018 * KO-IGF1: 0.002 *
ESV (µl)	51.2±7.3	47.5±7.8	46.1±14.6	63.1±28.4	WT-Con: 0.002 * WT-IGF1: 0.002* KO-Con: < 0.001 * KO-IGF1: < 0.001 *
LVAW,d (mm)	0.92±0.06	0.92±0.09	0.93±0.07	1.04±0.14	KO-IGF1: 0.030 *
LVAW,s (mm)	1.12±0.11	1.22±0.14	1.17±0.15	1.29±0.17	
LVID,d (mm)	4.25±0.33	4.30±0.33	4.06±0.53	4.26±0.63	WT-Con: 0.029 * WT-IGF1: 0.020*
LVID,s (mm)	3.32±0.36	3.26±0.32	3.16±0.66	3.34±0.94	WT-Con: < 0.001 * WT-IGF1: 0.003 * KO-Con: 0.002 * KO-IGF1: 0.005 *
LVPW,d (mm)	0.83±0.07	0.82±0.06	0.85±0.12	0.97±0.17	KO-IGF1: 0.002 *
LVPW,s (mm)	1.08±0.06	1.20±0.10	1.16±0.07	1.27±0.22	
LV mass (mg)	112.3±10.6	120.9±15.4	116.0±40.8	143.3±30.2	WT-IGF1: 0.006 * KO-Con: 0.006 * KO-IGF1: < 0.001 *

* p<0.05 vs pre-OP, # p<0.05 vs WT-Con, § p<0.05 vs WT-IGF1

Table S5: P-values from statistical tests (Fig. 1-6).

Figure	parameter	week 1	*p*-value	week 4	*p*-value
Fig. 1C	**EF**	Con	< 0.001 (vs. pre-OP)	Con	< 0.001 (vs. pre-OP)
		IGF1	0.009 (vs. pre-OP) < 0.001 (vs. Con)	IGF1	< 0.001 (vs. pre-OP) 0.006 (vs. Con)
Fig. 1D	**FAC**	Con	< 0.001 (vs. pre-OP)	Con	< 0.001 (vs. pre-OP)
		IGF1	0.016 (vs. pre-OP) < 0.001 (vs. Con)	IGF1	0.012 (vs. pre-OP) 0.002 (vs. Con)
Fig. 1E	**SV**	Con	< 0.001 (vs. pre-OP)	Con	< 0.001 (vs. pre-OP)
		IGF1	0.009 (vs. Con)		
Fig. 2A	**EF**	Con	< 0.001 (vs. pre-OP)		
		IGF1	0.005 (vs. pre-OP) < 0.001 (vs. Con)		

	parameter	segment	group	*p*-value
Fig. 2C	**Displ.- radial**	**Ant. free wall**	Con	< 0.001 (vs. pre-OP)
			IGF1	0.006 (vs. pre-OP) 0.006 (vs. Con)
Fig. 2D	**Strain - radial**	**Ant. free wall**	Con	< 0.001 (vs. pre-OP)
			IGF1	0.005 (vs. pre-OP) 0.041 (vs. Con)
Fig. 2E	**Strain - circumf.**	**Ant. free wall**	Con	< 0.001 (vs. pre-OP)
			IGF1	0.006 (vs. Con)
Fig. 2F	**Scar size**	0.03 (vs. Con)		

	parameter	region	*p*-value
Fig. 2H	**Capillary density**	Borderzone	0.003 (vs. Con)
		Scar area	0.037 (vs. Con)

Fig. 3B	**EF**	WT-Con	< 0.001 (vs. pre-OP)	WT-Con	< 0.001 (vs. pre-OP)
		WT-IGF1	0.028 (vs. pre-OP) 0.041 (vs. WT-Con)	WT-IGF1	0.034 (vs. pre-OP) 0.013 (vs. WT-Con)
		KO-Con	< 0.001 (vs. pre-OP)	KO-Con	< 0.001 (vs. pre-OP)
		KO-IGF1	< 0.001 (vs. KO-Con)	KO-IGF1	0.05 (vs. pre-OP) 0.003 (vs. KO-Con)
Fig. 3C	**FAC**	WT-Con	< 0.001 (vs. pre-OP)	WT-Con	< 0.001 (vs. pre-OP)
		WT-IGF1	0.026 (vs. WT-Con)	WT-IGF1	0.036 (vs. WT-Con)
		KO-Con	< 0.001 (vs. pre-OP)	KO-Con	< 0.001 (vs. pre-OP)
		KO-IGF1	< 0.001 (vs. KO-Con)		
Fig. 3D	**SV**	WT-Con	< 0.001 (vs. pre-OP)	WT-Con	< 0.001 (vs. pre-OP)
		KO-Con	0.015 (vs. pre-OP)	KO-Con	0.025 (vs. pre-OP)
		KO-IGF1	0.019 (vs. pre-OP)	KO-IGF1	0.013 (vs. pre-OP)

continued

continuation **Table S5**

		week 1	*p*-value	week 4	p-value
Fig. 4D	**EF**	WT-Con	< 0.001 (vs. pre-OP)	WT-Con	< 0.001 (vs. pre-OP)
		WT-IGF1	< 0.001 (vs. pre-OP) 0.012 (vs. WT-Con)	WT-IGF1	< 0.001 (vs. pre-OP) 0.009 (vs. WT-Con)
		KO-Con	< 0.001 (vs. pre-OP)	KO-Con	< 0.001 (vs. pre-OP)
		KO-IGF1	< 0.001 (vs. pre-OP) 0.002 (vs. WT-IGF1)	KO-IGF1	< 0.001 (vs. pre-OP) 0.005 (vs. WT-IGF1)
Fig. 4E	**FAC**	WT-Con	< 0.001 (vs. pre-OP)	WT-Con	< 0.001 (vs. pre-OP)
		WT-IGF1	0.001 (vs. pre-OP) 0.016 (vs. WT-Con)	WT-IGF1	< 0.001 (vs. pre-OP) 0.007 (vs. WT-Con)
		KO-Con	< 0.001 (vs. pre-OP)	KO-Con	< 0.001 (vs. pre-OP)
		KO-IGF1	< 0.001 (vs. pre-OP) < 0.001 (vs. WT-IGF1)	KO-IGF1	< 0.001 (vs. pre-OP)
Fig. 4F	**SV**	WT-Con	< 0.001 (vs. pre-OP)	WT-Con	< 0.001 (vs. pre-OP)
		KO-Con	0.008 (vs. pre-OP)	KO-Con	0.002 (vs. pre-OP)
		KO-IGF1	< 0.001 (vs. pre-OP)	KO-IGF1	0.001 (vs. pre-OP)
Fig. 5D	**CD206**	IGF1 (10 ng/ml)	0.018 (vs. untreated)		
		IGF1 (20 ng/ml)	0.024 (vs. untreated)		
Fig. 5E	**TNF-α**	M0+IGF1	0.028 (vs. M0)		
	MRC1	M0+IGF	0.035 (vs. M0)		
	IGF1	M0+IGF1	0.002 (vs. M0)		
Fig. 6B	**CD206$^+$**	IGF1	0.041 (vs. control)		

All P-values are rounded to three decimals. EF = ejection fraction, FAC = fraction area change, SV = stroke volume.

Table S6: Primer sequences

Gene	Primer sequence
Tumor Necrosis Factor Alpha	forward: GCCTCTTCTCATTCCTGCTTG reverse: CTGATGAGAGGGAGGCCATT
Interleukin 12A	forward: TACTAGAGAGACTTCTTCCACAACAAGAG reverse: TCTGGTACATCTTCAAGTCCTCATAGA
iNOS	forward: CATCAACCAGTATTATGGCTC reverse: TTTCCTTTGTTACAGCTTCC
Macrophage mannose receptor 1	forward: CTCTGTTCAGCTATTGGACGC reverse: CGGAATTTCTGGGATTCAGCTTC
Arginase 1	forward: CTCCAAGCCAAAGTCCTTAGAG reverse: AGGAGCTGTCATTAGGGACATC
Resistin-like alpha	forward: TCACAGGTCTGGCAATTCTTCTG reverse: TTTGTCCTTAGGAGGGCTTCCTCG
Insulin like growth factor 1	forward: CTGGACCAGAGACCCTTTGC reverse: GGACGGGGACTTCTGAGTCTT
Vascular Endothelial Growth Factor	forward: GCACATAGAGAGAATGAGCTTCC reverse: CTCCGCTCTGAACAAGGCT
Endoplasmic reticulum membrane protein complex 10	forward: GTCCCCTAAACAGCCACTCT reverse: CTCCTCCCAGAGTTCGGAAG
beta-Actin	forward: GATGTATGAAGGCTTTGGTC reverse: TGTGCACTTTTATTGGTCTC
Nuclear distribution C	forward: AGAACTCCAAGCTATCAGAC reverse: CTTCAGGATTTCCTGTTTCTTC
My-IGF1RKO	forward: TTCACCAGTACCATGGGCTCC reverse: CTTCAGCTTTGCAGGTGCACG